Heat and Moisture Budgets and Circulation Characteristics of a Frontal Squall Line

XIN LIN AND RICHARD H. JOHNSON

Department of Atmospheric Science, Colorado State University, Fort Collins, Colorado

(Manuscript received 2 July 1993, in final form 28 October 1993)

ABSTRACT

Heat and moisture budgets and mesoscale circulation features for the developing, mature, and dissipating stages of an intense frontal squall line that occurred in the central United States are investigated. The slow propagating behavior of the squall line made the dataset unique since observations covered a large fraction of the squall line life cycle. Budgets have been performed at six different times at intervals of 90 minutes using 1985 OK PRE-STORM rawinsonde data.

The squall line was followed by a low-level cold front. The flow pattern normal to the squall line was generally similar to previous squall line studies except that a low-level rear inflow associated with the cold front was superimposed upon expected squall line FTR/RTF (front to rear/rear to front) flows. The midlevel RTF flow was quite weak well behind the squall line during the developing and mature stages and significantly strengthened during the dissipating stage as the stratiform region developed, suggesting that internal processes within the expanding stratiform region played an important role in RTF flow development.

A convergence band resulting from system RTF and FTR flows extended upward and rearward from low levels near the leading edge of the system. During the developing and mature stages, peak convergence was located at low levels around the leading edge. At the dissipating stage, midlevel convergence behind the convective region intensified as the stratiform region developed, while low-level convergence near the leading edge gradually weakened.

Both the apparent heat source Q_1 and apparent moisture sink Q_2 showed an increasing upshear tilt when the stratiform region developed, as did the vertical velocity field. The system-averaged heating peak Q_1 was located at middle levels between 500 and 550 hPa throughout the evolution. The moisture sink Q_2 exhibited a single drying peak, which resulted from the convective region, at low levels around 700 hPa through most of the developing and early mature stages. During the late mature and dissipating stages, a double-peak structure in Q_2 became very pronounced. The coexistence of convective and stratiform drying appears to be the causal mechanism for the double peak in Q_2 at these stages. At later stages, a single drying peak resulting from the stratiform region was present at middle levels around 475 hPa.

1. Introduction

Observations in both midlatitudes and the tropics indicate that deep convection is usually organized into mesoscale features characterized by groups or bands of convective clouds and associated stratiform precipitation regions (e.g., Houze 1977; Zipser 1977; Houze et al. 1990). Latent heat released in these mesoscale convective systems (MCSs) plays an important role for the global general circulation. In earlier diagnostic studies of convective systems, due to temporal and spatial limitations of data, only the collective heating and moistening effects of many MCSs were evaluated (Reed and Recker 1971; Nitta 1972; Yanai et al. 1973).

With more field experiments and denser observational networks, MCSs could be properly partitioned into a convective region and a stratiform region (Houze 1977; Zipser 1977; Leary and Houze 1979; Houze et al. 1980; Johnson 1980; Leary and Houze 1980; Gamache and Houze 1982; Houze 1982; Johnson 1984). The vertical heating and moistening profiles, as well as mesoscale circulation features, display distinct differences between the convective region and the stratiform region. As Houze (1982) has pointed out, the total effect of the stratiform precipitation processes on the large-scale budget is heating of the middle to upper troposphere, where latent heating in the mesoscale updrafts is the dominant effect, and cooling in the lower troposphere, where melting and mesoscale downdraft evaporation dominate. In the convective region, latent heating dominates throughout the troposphere. As a mesoscale convective system evolves from the developing to mature to the dissipating stages, the total heating and moistening features vary as the stratiform region gradually expands.

Squall lines represent one common type of MCS with a relatively simple structure. Three main system-relative flows can be identified within squall lines evolution: a surface front-to-rear flow behind the leading

Corresponding author address: Mr. Xin Lin, Department of Atmospheric Science, Colorado State University, Fort Collins, CO 80523.

edge, a rear-to-front inflow at midlevels sloping down to the surface at the leading edge, and a front-to-rear flow originating at low levels in front of the leading edge and extending to the upper levels in the stratiform region. The rear-to-front flow (RTF) has been the subject of many studies (Hamilton and Archbold 1945; Newton 1950; Smull and Houze 1985, 1987; Rutledge et al. 1988; Zhang and Gao 1989; Schmidt and Cotton 1990; Weisman 1992). Not only is it directly associated with the formation of a surface wake low (Johnson and Hamilton 1988; Stumpf et al. 1991), but it also plays a significant role in the system maintenance (Smull and Houze 1985, 1987; Chong et al. 1987; Weisman et al. 1988; Rotunno et al. 1988; Lafore and Moncrieff 1989; Weisman 1992). However, whether it is generated by physical processes internal to the mesoscale system, by ambient RTF flow, or by other mechanisms is still not well understood. Smull and Houze (1987) suggested two mechanisms for the rear inflow circulations: 1) acceleration caused by the vertical flux of horizontal momentum in the convective line, and 2) a hydrostatically induced mesolow in the interior of the trailing stratiform region. Zhang and Gao (1989) found in their modeling study that the large-scale baroclinity provides a favorable RTF flow component. They emphasized the role of the upper-level jet in the formation of system RTF. Schmidt and Cotton (1990) proposed a gravity wave mechanism. They argued that the blocking of the flow aloft by convectively generated gravity waves and channeling of the flow below can lead to the development of the rear inflow jet. Experimental simulations by Weisman (1992) under a wide range of environmental factors indicate that the rear inflow is generated in response to the upshear tilting of the convective circulation, as the horizontal buoyancy gradients along the back edge of the expanding system create a circulation that draws midlevel air in from the rear.

Most of the previous squall line diagnostic studies were performed either over large temporal and spatial scales or at a specific stage of the system evolution. Studies covering a longer period of the life cycle of a squall line are quite rare. Therefore, the evolution and development of the heating, moistening, and mesoscale circulation features within a squall line are not well understood. On 26–27 June 1985 during the Oklahoma–Kansas Preliminary Regional Experiment for Storm-Central (PRE-STORM), a squall line followed by a low-level cold front passed through the PRE-STORM network. The squall line moved slowly and exhibited structural changes from the developing to mature to dissipating stages within the network. Trier et al. (1991) have studied the portion of this squall line that passed through Kansas and found that its precipitation structure and propagation characteristics were distinctly different from those of many previously observed cases. In particular, there were a series of rainbands forming parallel to and ahead of the cold front in an environment of moderate to large CAPE, small convective inhibition, and moderate, predominantly alongfront low-level shear. These rainbands, rather than forming in response to a squall line–induced cold pool, developed from in situ boundary-layer cloud streets and were likely aided in their formation by synoptic-scale geostrophic deformation with its associated mesoscale ascent along the cold front. After the collapse of the prefrontal rainbands, an intensification of the rear-inflow jet was observed in association with a broadening of the stratiform precipitation region.

The high-frequency soundings over the life cycle of the 26–27 June squall line provide the opportunity to assess the role of diabatic heating and its evolution in contributing to such features as the intensification of the rear-inflow jet. Moreover, the low-level cold front following the convective system may have imposed important forcing effects (Ogura and Portis 1984; Trier et al. 1991) on the evolution of this long-lived squall line that the sounding network may be able to detect. However, the specific role of the cold front in the squall line dynamics is not addressed in this paper.

In this study, heat and moisture budget analyses have been performed over an *extended period of the squall line life cycle:* at six different times at intervals of 90 minutes for the 26–27 June MCS as it traversed the PRE-STORM sounding network. Particular emphasis will be placed on the spatial and temporal evolution of mesoscale heating, moistening, and circulation features within the squall line as the stratiform region gradually developed. Possible mechanisms for the generation of the rear-to-front inflow will be discussed.

2. Budget equations and analysis methods

a. Heat and moisture budget equations

Budget equations for Q_1 (the apparent heat source) and Q_2 (the apparent moisture sink) (Yanai et al. 1973), with modifications to account for ice effects (Gallus and Johnson 1991), are defined by

$$Q_1 \equiv \frac{\partial \bar{s}}{\partial t} + \bar{\mathbf{v}}\cdot\nabla\bar{s} + \bar{\omega}\frac{\partial \bar{s}}{\partial p}$$
$$= Q_R + L_v(\bar{c} - \bar{e}) + (L_v + L_f)(\bar{d} - \bar{s}_*)$$
$$+ L_f(\bar{f} - \bar{m}) - \nabla\cdot\overline{s'\mathbf{v}'} - \frac{\partial}{\partial p}\overline{s'\omega'} \quad (1)$$

$$Q_2 \equiv -L_v\left(\frac{\partial \bar{q}}{\partial t} + \bar{\mathbf{v}}\cdot\nabla\bar{q} + \bar{\omega}\frac{\partial \bar{q}}{\partial p}\right)$$
$$= L_v(\bar{c} - \bar{e}) + L_v(\bar{d} - \bar{s}_*)$$
$$+ L_v\nabla\cdot\overline{q'\mathbf{v}'} + L_v\frac{\partial}{\partial p}\overline{q'\omega'}, \quad (2)$$

where $s = c_pT + gz$ is the dry static energy; q the specific humidity; Q_R the radiative heating rate; L_v and L_f the latent heats of vaporization and fusion; and c, e, d,

s_*, f, and m the condensation, evaporation, deposition, sublimation, freezing, and melting rates, respectively. The overbars refer to roughly 50 km × 50 km area averages, where primes denote subgrid deviations from the horizontal area average. The term Q_1 is a measure of radiative heating, latent heating from net condensation and ice phase changes, and the convergences of the vertical and horizontal eddy transports of sensible heat. Although the horizontal eddy flux is usually neglected in large-scale budget studies, it may be important in budget studies of squall lines (Gallus and Johnson 1991). However, there is no method to directly assess the importance of this term. Similarly, Q_2 is a measure of the net condensation and the horizontal and vertical convergences of the eddy moisture transports.

Spatial and temporal derivatives are calculated using a finite centered-difference method. Total divergence is computed using gridded wind data. Vertical velocities are calculated by integrating the mass continuity equation. A method proposed by O'Brien (1970) is used to adjust the vertical distribution of divergence and vertical velocity and make them satisfy continuity for the whole volume. Vertical velocities at the surface (975 hPa) and at the top (125 hPa) are set to zero. In their study of the 10–11 June 1985 case, Gallus and Johnson (1991) found that the influence of the topography on the calculation of the vertical velocity in the PRE-STORM area was very small and could be neglected when compared to the large magnitudes of the updrafts and downdrafts within the squall line system. Hence, topography is not considered in computing the vertical velocity in this case.

b. Data and analysis methods

Figure 1 shows the PRE-STORM sounding and radar network. In this study, PRE-STORM rawinsonde data from the NWS and supplemental sounding stations were used to perform heat and moisture budget calculations from 2100 UTC 26 June to 0430 UTC 27 June at intervals of 90 minutes.

There are eight rawinsonde release times at 90-min intervals used in this case. In order to decrease data spacing and better resolve the structural details of the squall line, a compositing technique was used in the budget calculations over 3-h periods centered at six different times (2100, 2230, 0000, 0130, 0300, 0430 UTC) ranging from the developing to mature to dissipating stages. Under the assumption of a quasi-steady-state squall line over 3-h intervals, the data at different times for one station are moved a distance ahead of or behind the actual position at centered times according to the average propagation speed of the system. The study by Trier et al. (1991) shows important changes in the structure of the convective line over short intervals (~1–2 h) during earlier times. However, after 2100 UTC, they found that the radar reflectivity pattern of the squall line became quite steady and there was

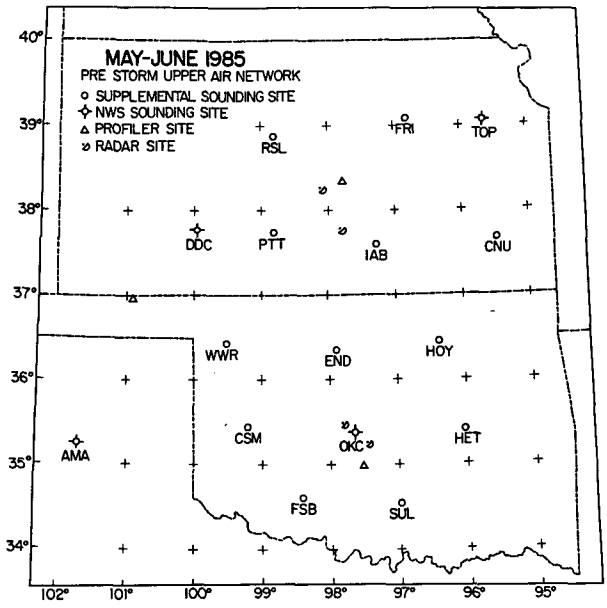

FIG. 1. The OK PRE-STORM observational mesonetwork (from Johnson and Hamilton 1988).

little evidence of the transient banded activity present earlier. Furthermore, since the emphasis in this study is on area-averaged rather than detailed features of the squall line structure, the compositing procedure for our purposes is regarded as reasonable. Thus, data at different times can be incorporated into a specific time so that more sounding data are available for the budget study. A comparison between composited and noncomposited fields has been performed. It is found that additional data under careful compositing significantly decrease the data spacing and can grasp more structural details in the squall line. However, the basic results are not qualitatively changed by the compositing procedure.

From 1930 to 2230 UTC, the average direction of the squall line was toward 132° and the average speed was about 5.0 m s^{-1} over Kansas and 7.0 m s^{-1} over Oklahoma. The speed gradually increased from 0000 to 0130 UTC. The maximum propagation speed was found at 0130 UTC. Over Kansas the average speed was 6.3 m s^{-1}, whereas over Oklahoma it was 8.6 m s^{-1}. The average movement of the squall line system during the mature stage in this case is smaller than that of the 10–11 June squall line, which had an average speed of 14 m s^{-1} from the mature to the dissipating stages (Rutledge et al. 1988; Gallus and Johnson 1991). The speed of the system decreased rapidly during the dissipating stage from about 5.0 m s^{-1} at 0300 UTC to 3.4 m s^{-1} at 0430 UTC and 1.0 m s^{-1} at 0600 UTC. Due to the slow movement at 0600 UTC, the compositing technique was not applied because it produced unrealistic gradients in the analyzed fields.

The sounding stations within the PRE-STORM rawinsonde network have an average spacing of about

160 km. After the compositing technique was applied, the average spacing between stations decreased and the total number of sounding stations available for objective analysis at individual times increased from about 15 to more than 30 except at 0600 UTC.

For this budget analysis, sounding data were vertically interpolated from 975 hPa to 125 hPa at intervals of 25 hPa. Hydrostatic and horizontal checks were performed to eliminate erroneous sounding data. Balloon drift was also considered during data processing. A 1–2–1 smoothing scheme was used to filter out small-scale disturbances in the vertical.

The domain selected in the budget study is from 33° to 40°N and from 94° to 102°W. A Barnes objective analysis scheme (Barnes 1964) in spherical coordinates was used to interpolate the sounding data onto a 0.5° by 0.5° grid. Radar maps showed that from 1930 to 2230 UTC, the entire width of the squall line was about 90 km. The width increased to 110 km from 0000 to 0130 UTC and reached 150 km during the dissipating stage (0300 to 0600 UTC). Due to the slow movement and the narrowness of the squall line and the distribution of stations, the composited rawinsonde stations were not evenly distributed. The average distances between sounding stations ranged from 50 to 90 km at lower levels. A filter response of about 50 percent at 100 km was selected at levels below 400 hPa. Due to the missing data at higher levels, the average station spacing increased and the response function was selected to represent a horizontal scale of about 200 km above 400 hPa. Unlike the 10–11 June case, which had a trailing stratiform region 160 km wide, both the convective and stratiform regions in the 26–27 June case were about 40 to 60 km wide during the developing and mature stages; therefore, the stratiform region at these times was not as accurately represented by the objective analysis scheme as in the 10–11 June case. Because smaller-scale motions could not be resolved and the features in both the convective region and the stratiform region were smoothed into each other and into the environment, diagnostic variables such as the vertical motion contained considerable aliasing. Ogura and Liou (1980) and Kuo and Anthes (1984) pointed out this common problem in mesoscale analyses. During the dissipating stage, the horizontal extent of the stratiform region increased to 100 km, so that its structural details could be better resolved during that stage.

Although the budget study emphasizes the upper-air sounding data, radar maps and surface rainfall data are also used. Radar reflectivity maps from the NWS WSR-57 radars located at Wichita, Kansas, and Oklahoma City, Oklahoma, indicated the evolution of the reflectivity patterns of the 26–27 June squall line from the developing to mature to dissipating stages. Values of radar reflectivity $\leq$ 35 dBZ just behind the convective line are used to separate the system into the convective and stratiform regions. The stratiform region designation was assigned only when there was an ~50 km or greater region of weaker reflectivity. In addition, surface rainfall rates and transition zone (weak reflectivity region behind the convective line at the dissipating stages) are used to assist in this determination.

3. Mesoscale structure

a. Squall line history

In Fig. 2, the surface pressure analysis for 1200 UTC 26 June 1985 is presented to illustrate the location of the cold front extending from the western Great Lakes to New Mexico. A rather pronounced temperature contrast existed across this front. The reader is referred to Trier et al. (1991) for additional background information on the synoptic situation for this case.

Before 2100 UTC 26 June, the mesoscale convective system was somewhat disorganized. Figure 3a shows the composited low-level radar reflectivity at 1920 UTC. The system at this time can be divided into three distinct components (Trier et al. 1991): a prefrontal squall line 50 to 70 km wide (center band in Fig. 3a), a narrow rainband coincident with the surface cold front (westernmost band), and a series of convective

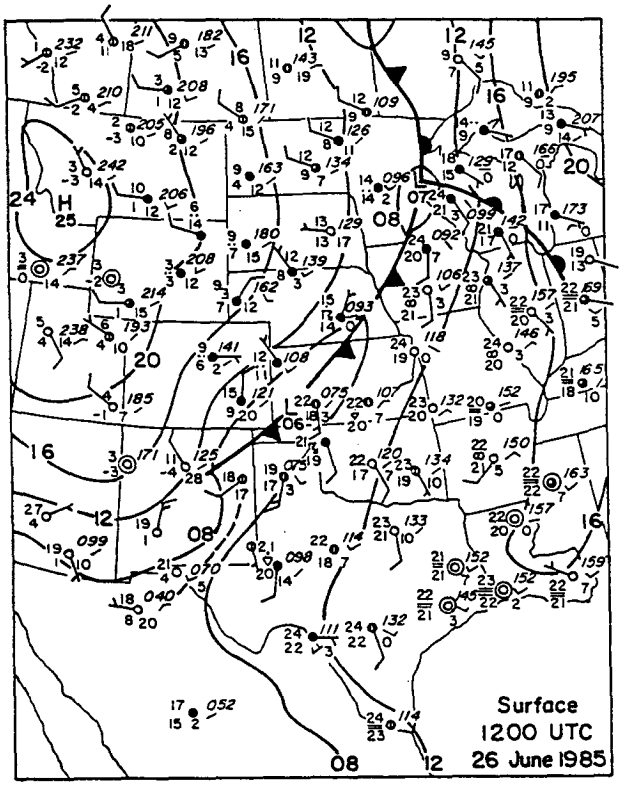

FIG. 2. NMC surface pressure analysis for 1200 UTC 26 June 1985 (from Trier et al. 1991). Conventional station model is used with temperatures and dewpoints expressed in degrees Celsius. A full barb on the wind flags indicates a speed of 5 m s^{-1}.

rainbands and cells that formed in advance of the prefrontal squall line. With the passage of time, the entire squall line system gradually consolidated into a more prominent single band (Fig. 3b), although some presquall convection still existed. The cold front and frontal rainband slowly caught up with the prefrontal squall line and the reflectivity increased, especially over the Oklahoma region. The convective rainbands and cells ahead of the prefrontal squall line also slowly merged with the squall line (Figs. 3b and 3c) and redefined the leading edge of the MCS (Trier et al. 1991). An example of the distribution of composited stations used in subsequent analyses is shown in Fig. 3c.

During the intensive analysis from 2100 UTC 26 June to 0430 UTC 27 June (Figs. 3b–g), the portion of the 26–27 June squall line over Kansas had distinct differences from the part over the Oklahoma region. Although considerable deep convection occurred earlier (Trier et al. 1991), the radar echo over Kansas from 2100 to 0400 UTC was dominated by low reflectivity, indicating stratiform precipitation. However, during the first part of this period, there were convective bands ~10–20 km wide at the leading edge. After 0400 UTC, most of the radar echo over the Kansas region dissipated.

From 2130 to 0000 UTC (Figs. 3b, 3c, and 3d), the Oklahoma portion had higher radar reflectivity than in Kansas and the convective region was equal to or larger than the area occupied by the stratiform region. During this interval, this segment of the squall line is defined as being in its developing and early mature stages. Beginning at 0130 UTC (Fig. 3e), the width of the stratiform region gradually increased from about 30–40 km to nearly 100 km at later times (Figs. 3g and 3h). After 0430 UTC 27 June, the movement of the squall line nearly ceased but its dissipation continued.

Since the squall line exhibited alongline asymmetric features and the widths of the stratiform and convective regions varied at different times and in different regions, vertical cross sections were constructed using a method somewhat different from that used by Ogura and Liou (1980) and Gallus and Johnson (1991). In this study, slabs (~50 km wide) were selected normal to the squall line instead of along the squall line. The area-averaged vertical cross sections were then determined by averaging these slabs between the two dashed lines on each of the radar maps (Fig. 3). It is acknowledged that considerable variability exists along the squall line segment used for averaging. However, the resolution of the soundings is not sufficient to document this variability at all times, so the emphasis here will be on line-averaged values (except at 2230 UTC, when vertical motion results for the Kansas and Oklahoma portions of the squall line segment will be shown separately; see Fig. 3c).

b. Relative wind

The vertical cross sections of relative wind normal to the squall line from 2100 UTC 26 June to 0430 UTC 27 June are shown in Fig. 4 at 90-min intervals. Heavy solid lines are isentropes of 300 and 305 K, approximately delineating the low-level frontal zone. The relative velocity is obtained by subtracting the average movement of the system from gridded wind data normal to the line.

At 2100 UTC (Fig. 4a), a FTR flow is quite evident ahead of the system. The peak value (about 12.0 m s^{-1}) was slightly above 900 hPa and was much weaker than that found in the 10–11 June case (nearly 24.0 m s^{-1} at 900 hPa) (Gallus and Johnson 1991). The FTR flow sloped upward toward the rear of the system with speeds exceeding 24.0 m s^{-1} over 200 km behind the leading edge between 250 and 300 hPa, similar to that of the 10–11 June case. The strong gradient in FTR flow above the leading edge from 300 to 200 hPa is a reflection of strong divergent outflow at upper levels.

The most pronounced difference from the 10–11 June squall line is that a strong RTF flow (up to 7 m s^{-1} near 850 hPa) occurred at low levels behind the leading line in the 26–27 June case. In the 10–11 June case, an RTF flow extended from roughly 500 mb behind the stratiform region to 800 mb within the stratiform precipitation region. It appears that the low-level RTF flow in the 26–27 June case was associated with the frontal circulation. There was also a weak midlevel RTF flow that can be observed near 600 hPa, but it did not extend forward into the system.

Relative wind at 2230 and 0000 UTC (Figs. 4b and 4c) showed similar patterns to that of 2100 UTC, except that the lower branch of the RTF flow gradually extended forward to within 50 km of the leading edge. This behavior is likely a reflection of the fact that the cold front moved a little faster than the squall line. During this time interval, the system-averaged vertical cross sections showed that there was still no tendency for the midlevel RTF inflow to extend forward in a pronounced way into the system. In contrast, Trier et al. (1991) showed a downward and forward extending RTF flow in a vertical cross section constructed from radar data over Kansas, where the stratiform region dominated. However, the results of our study are most heavily influenced by the portion of the line to the south, where the stratiform region was far less extensive. Also at these times, weak FTR flow can be seen at low levels behind the leading convective line as has been found in other studies (Srivastava et al. 1986; Augustine and Zipser 1987; Smull and Houze 1987; Johnson and Hamilton 1988; Rutledge et al. 1988; Gallus and Johnson 1991).

By 0130 UTC (Fig. 4d), the depth of the RTF flow within 200 km behind the leading edge began to increase. Not only was there a peak (more than 4.0

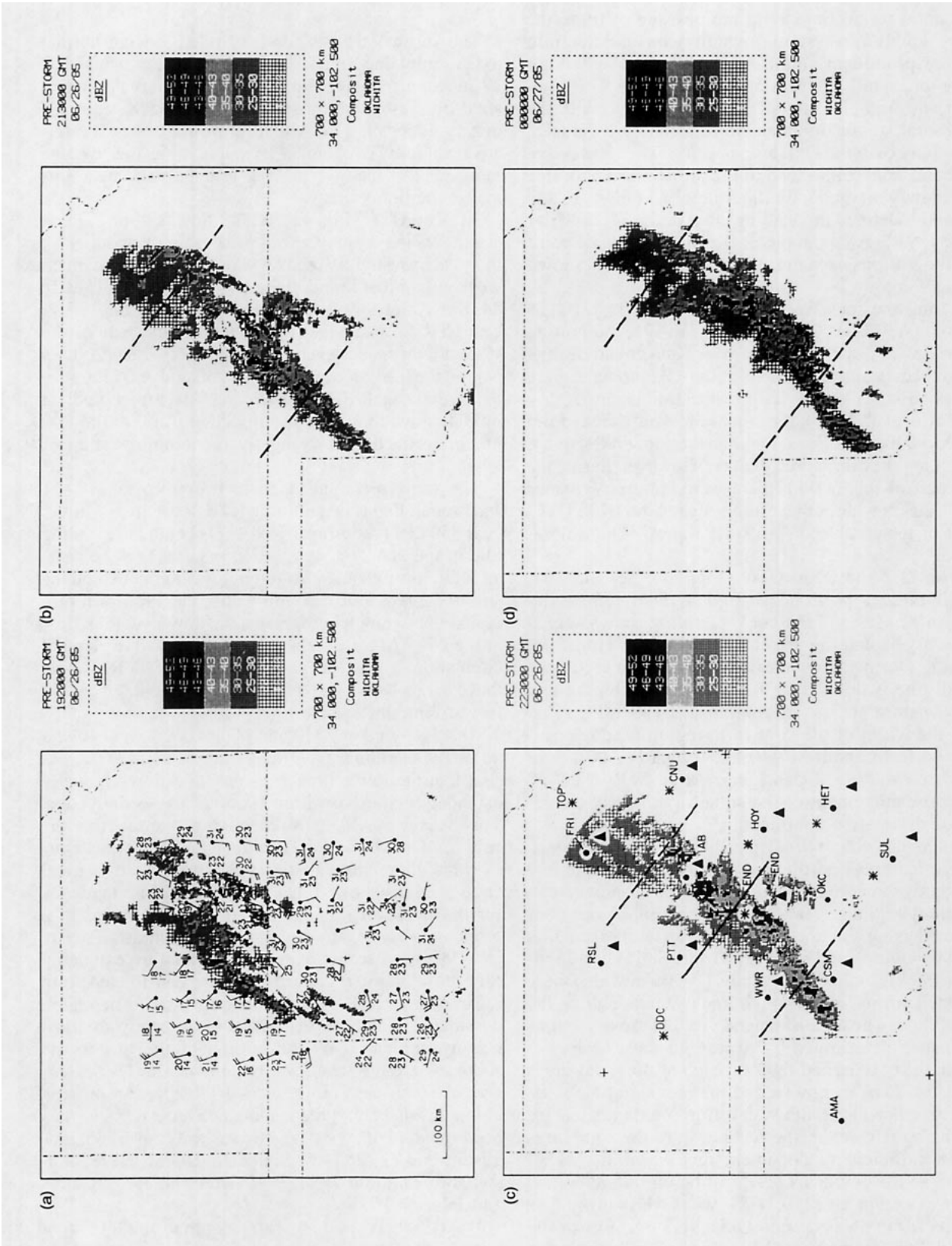

FIG. 3. Composited low-level reflectivity patterns during the lifetime of the 26–27 June squall line. (a) 1920 UTC, (b) 2130 UTC, (c) 2230 UTC, (d) 0000 UTC, (e) 0130 UTC, (f) 0300 UTC, (g) 0430 UTC, and (h) 0600 UTC. Data in the region between two dashed lines were used to construct area-averaged vertical cross sections.

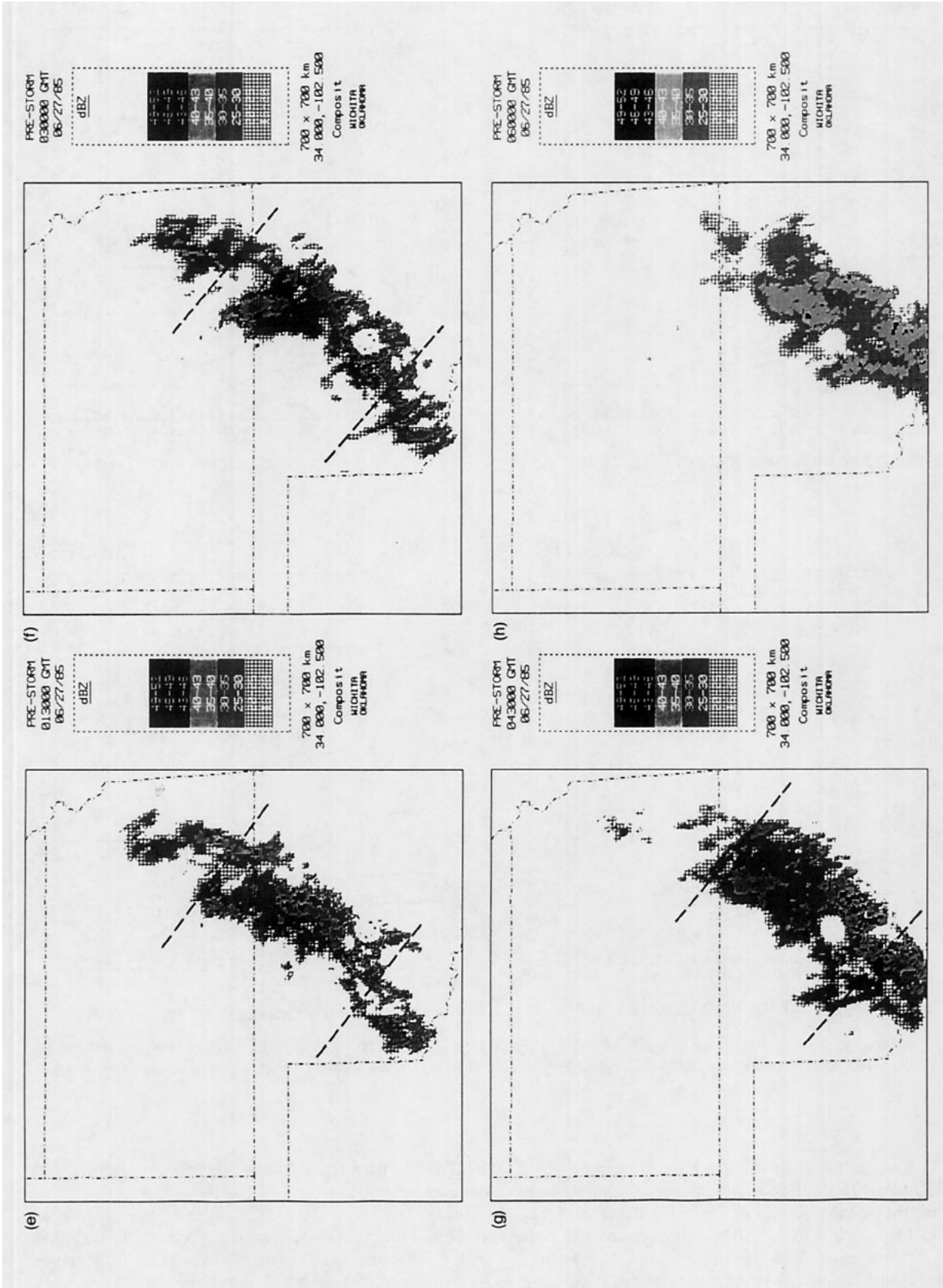

FIG. 3. (*Continued*) Shown in Fig. 3a are surface winds (one full barb: 5 m s^{-1}) and surface temperature and dewpoint in degrees Celsius. Positions of composited sounding data at 2230 UTC are shown in Fig. 3c. Asterisks and triangles refer to 90-min sounding positions after and prior to, respectively, the central time. Heavy line in Fig. 3c defines areas used for Kansas and Oklahoma composites shown in Figs. 9a,b.

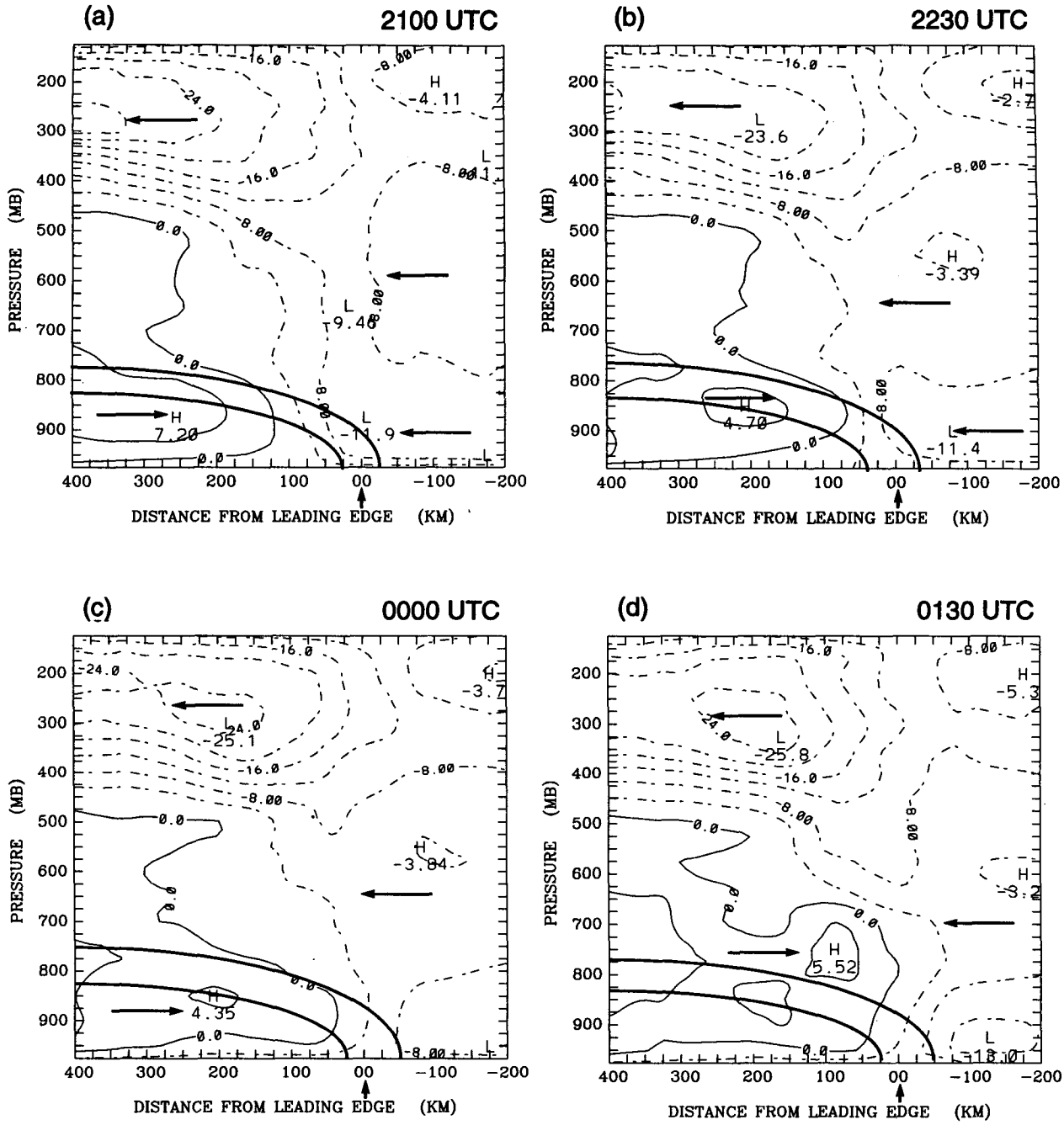

FIG. 4. Relative wind (in m s^{-1}) normal to the squall line. (a) 2100 UTC, (b) 2230 UTC, (c) 0000 UTC, (d) 0130 UTC, (e) 0300 UTC, and (f) 0430 UTC. Positive values indicate flow from rear to front (left to right). Heavy solid lines approximately delineate the low-level

m s^{-1}) associated with the cold front between 900 and 850 hPa 175 km behind the system, but also there was another peak (nearly 5.5 m s^{-1}) located at 750 hPa 75 km behind the leading edge. Since the cold front did not extend to this height at this position, this maximum is probably an indication that the mid-level RTF flow had finally developed behind the system.

From 0300 to 0430 UTC (Figs. 4e and 4f), when the squall line was in its dissipating stage, the RTF flow shows different patterns from those of the early stages. At a distance of over 400 km behind the leading edge,

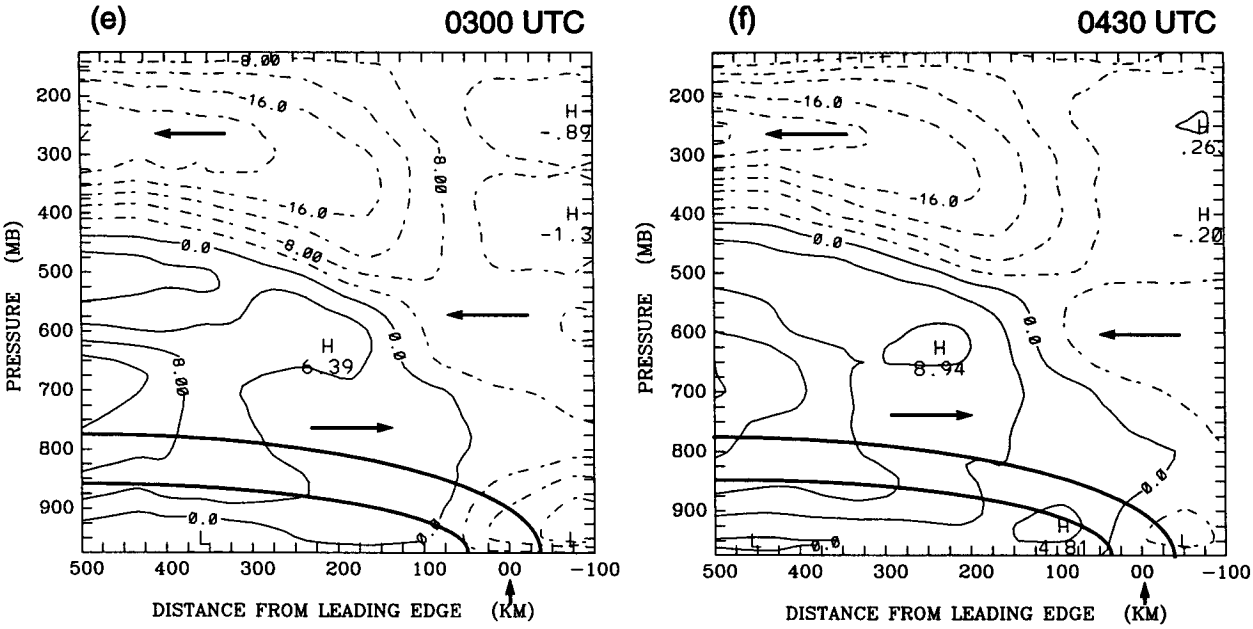

FIG. 4. (*Continued*) frontal zone represented by the 300-K and 305-K isentropes. Short arrow at bottom denotes the leading edge.

the RTF inflow intensified, increasing to 12.0 m s^{-1} between 600 and 800 hPa 500 km behind the leading edge. Within 300 km of the convective line, there were two clearly separated branches of RTF flow at 0300 UTC. The upper branch showed a clear pattern of the strengthening midlevel RTF flow extending from well behind the leading edge into the system. This strengthening also corresponded to the period when the trailing stratiform region expanded significantly (Figs. 3f–g).

The above analyses indicate there are some similarities and some differences between the 26–27 June squall line and the 10–11 June case. A basic difference was that the 26–27 June squall line was followed by a low-level cold front and its associated RTF flow had a peak of 5 to 8 m s^{-1} near 800–950 hPa. The midlevel RTF flow associated with the squall line system was not prominent during the early stages when the stratiform region was narrow [an exception is outside of our analysis domain over northeastern Kansas, where the stratiform region and rear inflow developed at an earlier time (Trier et al. 1991)]. From the mature to the dissipating stages, coincident with the expansion of the stratiform region over Oklahoma, the midlevel RTF flow significantly strengthened to the rear of the stratiform precipitation region. Eventually, the two RTF inflows, resulting from different mechanisms, formed a deep layer of RTF inflow behind the leading edge. Examination of geopotential height fields at 600 hPa (near the melting level) (Fig. 5) indicates that at the early mature stage (0000 UTC; Fig. 5a), over north-central Oklahoma and south Kansas, a weak trough began to develop within the MCS. At 0430 UTC (Fig. 5b), a deep mesolow developed within the MCS and coincided well with the expanding stratiform region over Oklahoma (Fig. 3g). A mesoscale high was present to the rear of the squall line. A momentum budget study of the squall line (Lin 1992) indicates that the couplet of the mesolow and mesohigh explains most of the dramatic strengthening of the midlevel RTF flow at the back edge of the squall line during the dissipating stage. Since the strengthening midlevel RTF flow did not appear to be linked with a descending upper-level jet [in contrast to the June 10–11 case (Zhang and Gao 1989; Gallus and Johnson 1991)] and the rear-inflow jet and midlevel mesolow only became prominent as the stratiform region developed, it appears that the midlevel RTF flow may have been generated by the physical processes internal to the stratiform region (Smull and Houze 1987; Trier et al. 1991; Weisman 1992).

c. *Divergence*

Figure 6 illustrates the vertical cross sections of divergence normal to the 26–27 June squall line at 0000 and 0430 UTC, which represent the early mature stages and dissipating stage, respectively. The strongest convergence was generally located at about 900 hPa near the leading edge of the front during the developing/mature stages (Fig. 6a). Similar to previous diagnostic studies of middle-latitude squall lines (Ogura and Liou 1980; Gallus and Johnson 1991), the axis of the convergence within the system tilted from low levels near the leading edge up to high levels in the rear of the system due to the convergence of the RTF and FTR

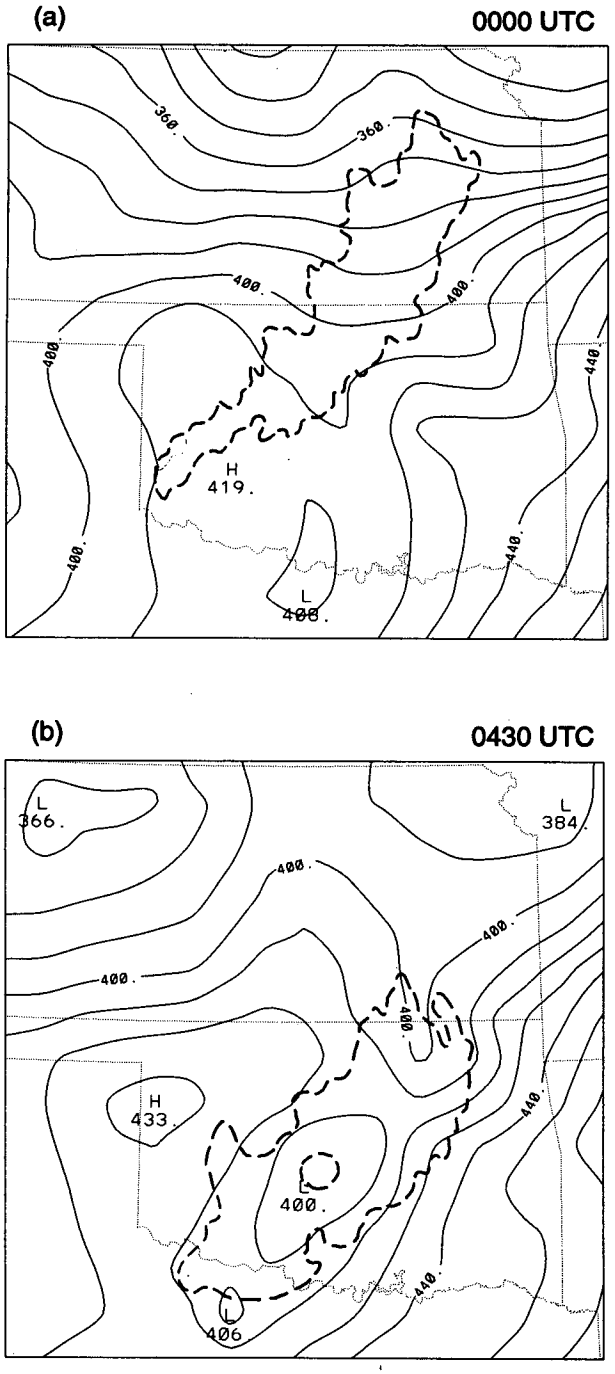

FIG. 5. Geopotential height at 600 hPa in the PRE-STORM region for (a) 0000 UTC, (b) 0430 UTC. Heights are expressed in meters above 4000 m. Dashed line encloses squall line precipitation region.

flows. At the dissipating stage (Fig. 6b), the low-level convergence decreased and the peak convergence was located near 600 hPa. This increase at middle levels at later times is an indication of a strengthening of the rear-inflow jet at the same time as an expansion of the stratiform region (Figs. 3f–h, 4e–f).

Figure 7 shows the vertical profiles of divergence averaged over the convective and stratiform regions. In the convective region (Fig. 7a), the vertical profiles at different times (from 2100 to 0300 UTC) were quite similar. Convergence was present below 550 hPa with the peak values generally located at ~850–950 hPa, which fed deep convective updrafts, similar to the results found by Gamache and Houze (1982) in a study

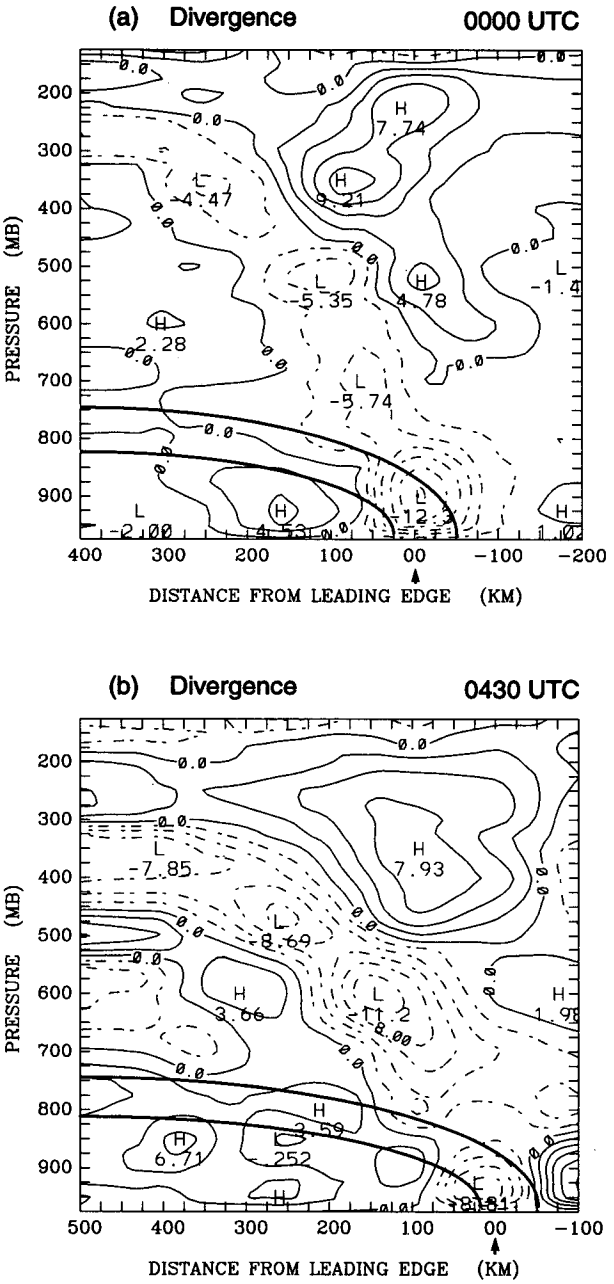

FIG. 6. Divergence (in 10^{-5} s^{-1}) normal to the squall line. (a) 0000 UTC, (b) 0430 UTC. Heavy solid lines approximately delineate the low-level frontal zone.

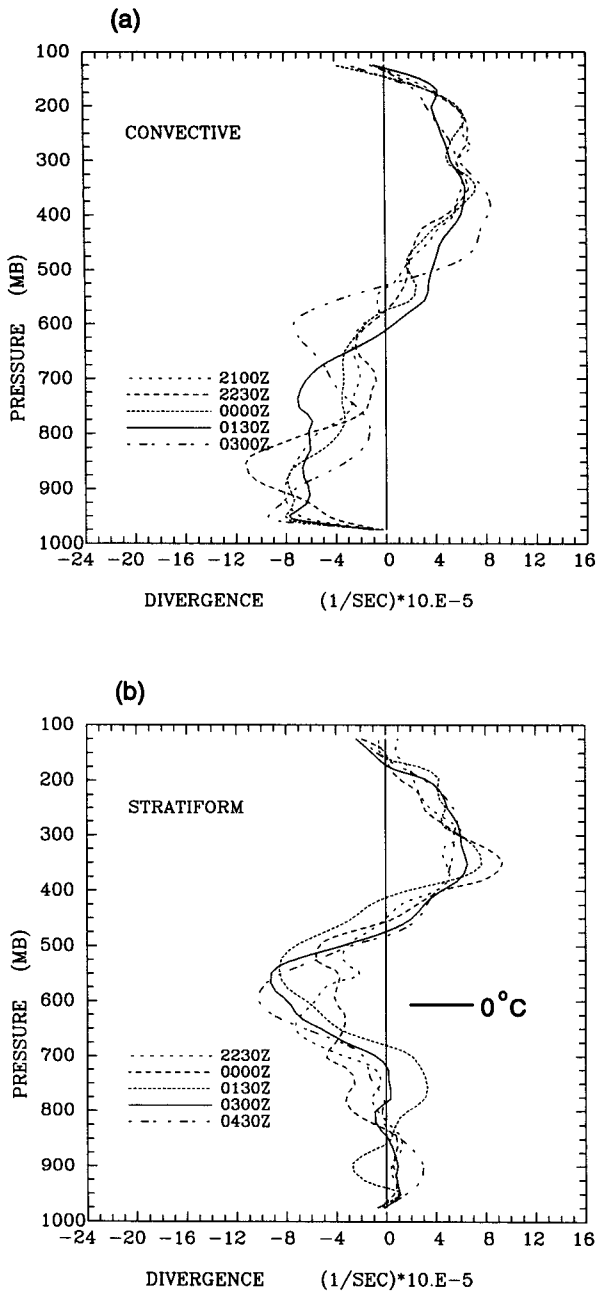

FIG. 7. Vertical profiles of divergence (in 10^{-5} s^{-1}) averaged over (a) the convective region from 2100 to 0300 UTC and (b) the stratiform region from 2230 to 0430 UTC.

of a tropical squall line. Above 550 hPa, divergence associated with outflow from the cells dominated.

The vertical profiles of divergence in the stratiform region (Fig. 7b) showed a different pattern from the convective region. Although there may be aliasing from the convective region, divergence generally occurred at low levels below 825 hPa. This feature is a reflection of the system's mesoscale downdrafts. Convergence peaks were generally located between 500 and 600 hPa (near the melting level) and the magnitudes increased with time, consistent with the expansion of the stratiform region. This convergence is manifested in Fig. 4 as opposing FTR and RTF flows. Between 175 and 400 hPa, divergence occurred due to outflow at the top of the system. The stratiform region divergence profiles in Fig. 7b closely resemble those shown by Trier et al. (1991, their Fig. 22) deduced at 0300 UTC over Kansas.

The evolution of divergence profiles for the entire system is considered in Fig. 8. The shaded region represents convergence values larger than 4×10^{-5} s^{-1}. As the system evolved from the developing to mature to dissipating stages, the low-level peak convergence (near 900 hPa) gradually decreased, indicating decreasing boundary-layer supply of mass and moisture to the whole system. On the other hand, the midlevel convergence gradually increased, implying a growing influence of the stratiform region. More mass converged at midlevels by the RTF and FTR flows during the later stages and fed mesoscale updrafts and downdrafts within the stratiform region (shown later). The midlevel convergence at later stages peaked near the 0°C level (600 hPa, Fig. 7b), suggesting that cooling from melting may have enhanced inflow into the system. From 500 to 150 hPa, a deep layer of divergence existed within this volume, increasing from the developing to mature stages and decreasing at the dissipating stage.

d. Vertical motion

Figure 9 shows the vertical motion in the squall line from the developing and mature through the dissipating

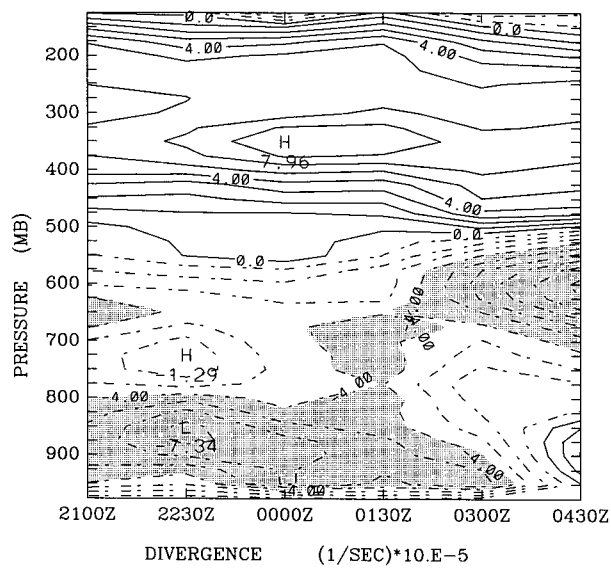

FIG. 8. Time series of divergence (in 10^{-5} s^{-1}) averaged over the entire system from 2100 to 0430 UTC. The shaded region represents convergence values larger than 4×10^{-5} s^{-1}.

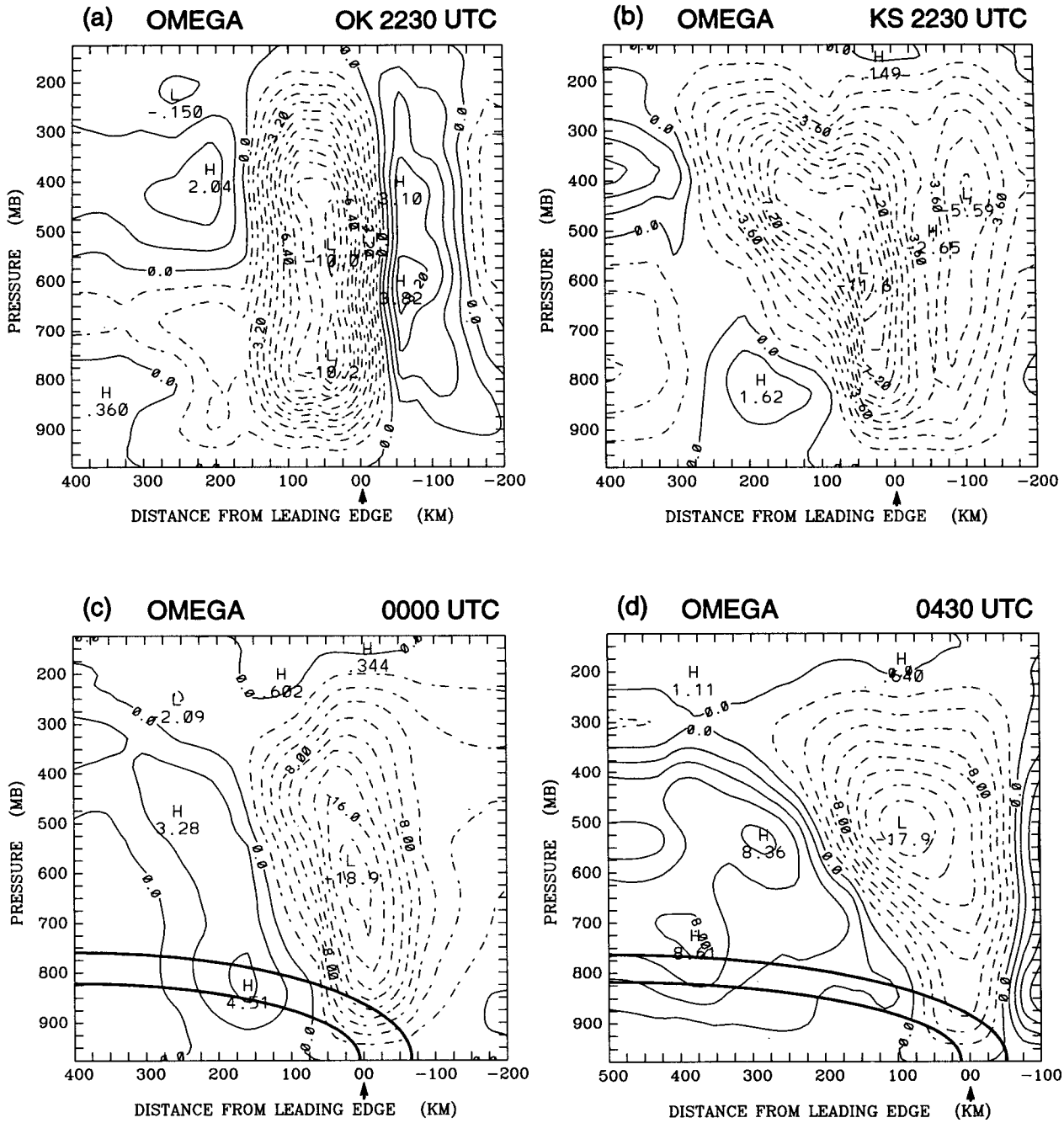

FIG. 9. Vertical velocity (ω) (in units of μb s^{-1}) normal to the squall line over (a) the OK region at 2230 UTC, (b) the KS region at 2230 UTC, (c) 0000 UTC, and (d) 0430 UTC.

stages. During the early stages (such as 2230 UTC), the 26–27 June squall line demonstrated the most pronounced asymmetry between the Oklahoma and Kansas regions. Since the vertical motion field reflects this asymmetry, cross sections for the Kansas and Oklahoma portions of the line segment in Fig. 3c are portrayed separately. At 2230 UTC, the precipitation associated with the squall line over Oklahoma was mostly convective (about 30 to 50 km wide, Fig. 3c). The vertical velocity within this part of the squall line was dominated by upward motion throughout the whole troposphere with a peak at 550 hPa at 2230 UTC (Fig. 9a). Because of the narrowness of the squall line, aliasing due to poor resolution, and the weaker intensity

of the squall line, the magnitude of upward motion was much smaller than that found by Gallus and Johnson (1991) for the 10–11 June case.

Regions of compensating descent in front of the leading edge have been shown in many squall line studies (Fankhauser 1974; Sanders and Paine 1975; Gamache and Houze 1982; Gallus and Johnson 1991; Biggerstaff and Houze 1991). Ahead of the leading edge of the 26–27 June squall line, there was a wide region of downward motion throughout the depth of the troposphere over Oklahoma. At upper levels to the rear of the system, there was another extensive region of compensating downward motion with a peak centered around 400 hPa.

Based on radar reflectivity maps and surface precipitation (Lin 1992), the part of the squall line over Kansas was in its mature to dissipating stages at 2100 and 2230 UTC. Correspondingly, the pattern of the vertical motion (2230 UTC, Fig. 9b) was distinctly different from that over Oklahoma. The most prominent difference was the larger horizontal extent of upward motion over Kansas. Near the leading convective line, there was upward motion throughout most of the troposphere with an average peak near 600 hPa. In the stratiform region, from middle to upper levels there was upward motion peaking near 450 hPa. At low levels from 800 hPa to the surface, weak downward motion can be seen at 100 to 300 km behind the leading edge. Because the rear of the system was near the northwest edge of the grid, the features within the stratiform region were smoothed to the rear of the system. Also the weak upward motion ahead of the leading edge might be the result of aliasing of the features in the convective region during objective analysis since the leading edge of the system over Kansas was near the east side of the sounding network.

Vertical motion averaged over the indicated area (Fig. 3d) at the mature stage at 0000 UTC is shown in Fig. 9c. The slopes of the axis of maximum upward motion and downward motion were nearly vertical. This structure is in agreement with radar observations showing that the stratiform region was still quite narrow and the system was not expanding rapidly. The peak of upward motion was located at about 550 to 600 hPa near the leading edge. To the rear of the system, there was a deep layer of downward motion with a peak around 800 hPa.

At the dissipating stage (0430 UTC, Fig. 9d), strong downward motion can be clearly seen to the rear of the system. The interface between downward and upward motion became more horizontal as the stratiform region expanded, consistent with the observations of Zipser (1988) and Klimowski (1994), and modeling studies of Lafore and Moncrieff (1989) and Weisman (1992). Downward motion also occurred ahead of the system, which may have resulted from the compensating flow associated with the MCS.

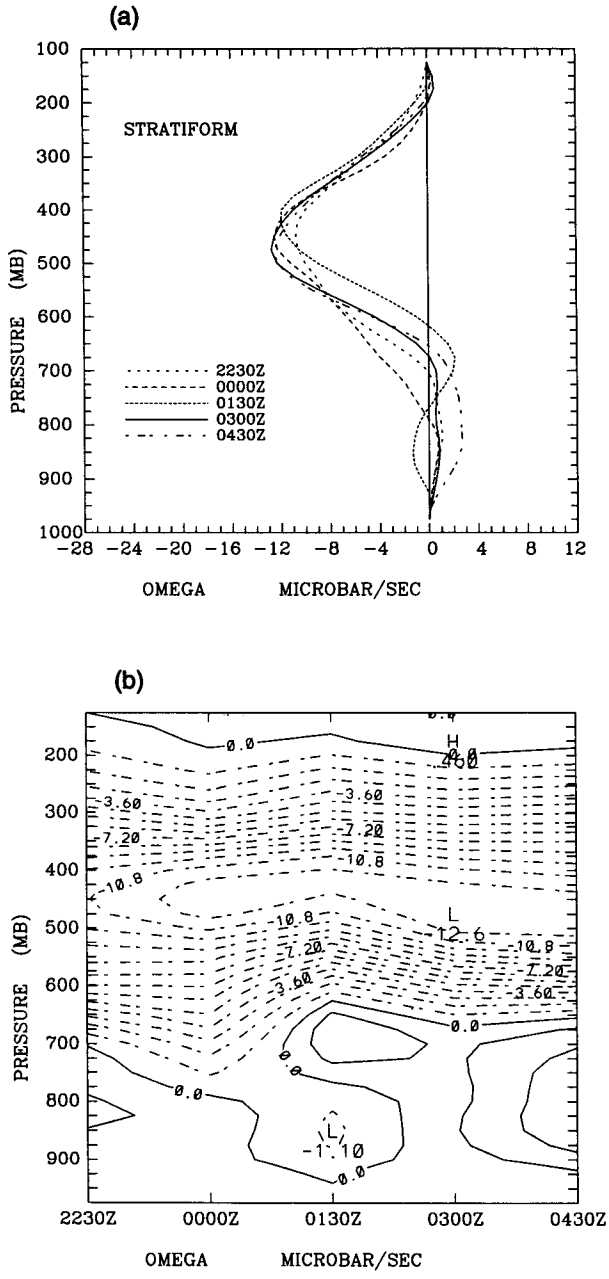

FIG. 10. Vertical profiles (a) and time series (b) of vertical motion ($\mu b\ s^{-1}$) averaged over the stratiform region of the squall line at different budget times from 2230 to 0430 UTC.

Figure 10 shows the vertical profiles and evolution of the vertical motion in the stratiform region averaged over both Kansas and Oklahoma. Vertical motion above the melting level between 600 and 250 hPa was dominated by mesoscale ascent in the anvil cloud. The level of maximum ascent was located at about 450 hPa. At low levels, weak downward motion generally dominated and the depth and magnitude of descent gradually increased as the stratiform region expanded. The

magnitude of the mesoscale downdraft in the relatively narrow stratiform region is likely underestimated due to aliasing from the convective region.

Figure 11 shows the vertical profiles and evolution of vertical velocity averaged over the entire system. From 2100 to 0130 UTC, the vertical profiles were quite similar to each other with peak upward motion over 15.0 μb s^{-1} centered around 500 hPa. Prominent changes took place during the dissipating stage when the developing stratiform region imposed more influence on the squall line. As illustrated in Fig. 4f, the RTF flow descended from 200 km behind the leading edge into the system, and the mesoscale downdrafts gradually strengthened as the stratiform region developed. The upward motion at low levels during the dissipating stage rapidly decreased. At 0430 UTC, the system-averaged vertical motion was generally downward below 750 hPa. Weak downward motion was also present at the top at some times, similar to the results found by Balsley et al. (1988), Houze (1989), and Johnson et al. (1990). This feature may reflect sinking along the top of the stratiform region, perhaps as a result of radiative cooling and/or flow along isentropes that have deformed upward by the upward motion in the convective line (Johnson et al. 1990).

The kinematic analyses indicate that the stratiform region played an essential role in the development of mesoscale circulation features. The strengthening of the midlevel RTF flow, the appearance of a midlevel mesolow behind the convective region and mesohigh to the rear of the line, the midlevel convergence peak behind the convective region, and the increasing tilt of the upward/downward motion couplet were all closely associated with the expansion of the stratiform region. It is proposed that these mesoscale circulation features were generated by the internal processes within the stratiform region (e.g., Smull and Houze 1987; Lafore and Moncrieff 1989; Trier et al. 1991; Weisman 1992). Another unique feature is that there was a low-level RTF flow induced by the cold front superimposed upon the expected system RTF/FTR flows. The cold front catching up with the leading convective line during the early stages may have contributed to the upshear tilting of the convective circulation, which may have also contributed to inducing the RTF inflow (Weisman et al. 1988).

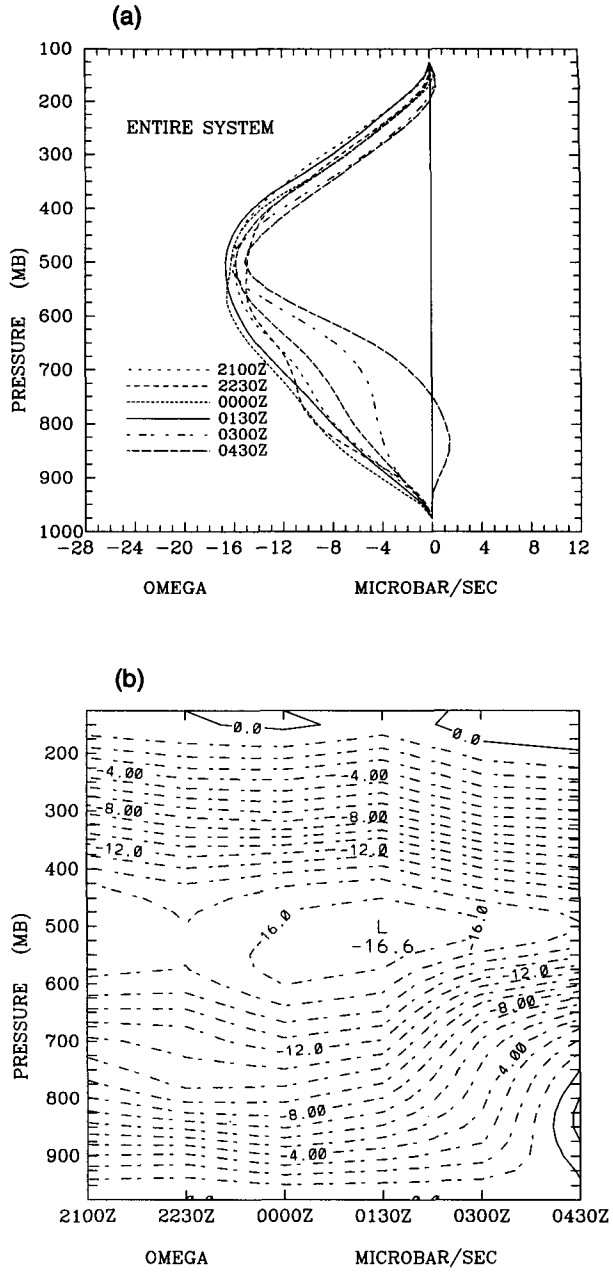

FIG. 11. Vertical profiles (a) and time series (b) of vertical motion (μb s^{-1}) averaged over the entire squall line system at different budget times from 2100 to 0430 UTC.

4. The heat and moisture budgets

a. Spatial and temporal evolution of the heat budget

The area-averaged vertical cross sections of Q_1 at 0000 and 0430 UTC are illustrated in Fig. 12. The approximation of $Q_1 \propto -\bar{\omega}$ is quite evident in this case (cf. Figs. 9 and 12), similar to the results found by Houze (1982) and Johnson and Young (1983). The maximum heating rate at 0000 UTC was located at about 525 hPa (Fig. 12a). In agreement with the observation showing that the stratiform region remained narrow, the tilting of the vertical heating band was very small. At 0430 UTC (Fig. 12b), the maximum heating rate decreased and the tilting of the vertical heating band became apparent as the stratiform region developed. At the back edge of the squall line, mesoscale cooling occurred through nearly the whole depth of the troposphere. At 0000 UTC, there were two cooling peaks to the rear of the system at middle and low levels,

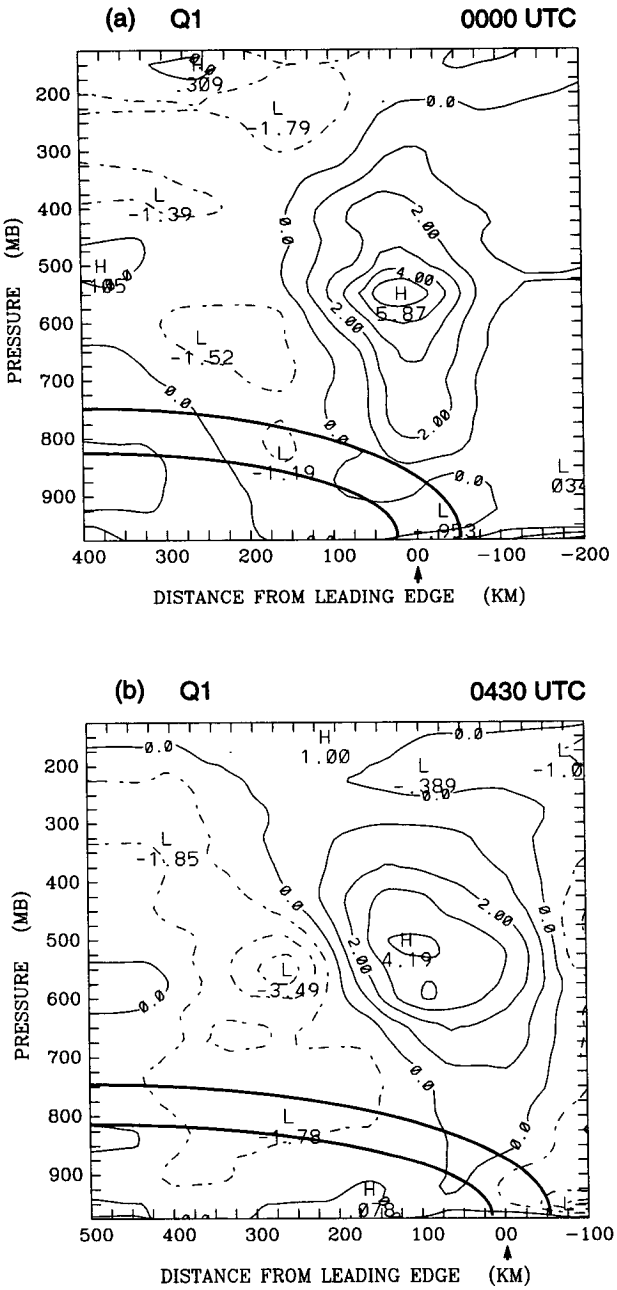

FIG. 12. Apparent heat source Q_1 (°C h^{-1}) at (a) 2230 UTC, (b) 0430 UTC.

respectively. As time progressed, the cooling rate of the higher peak increased and the level rose from 650 hPa to 550 hPa.

Figure 13 shows the vertical profiles of Q_1 and the evolution in the convective region from 2100 to 0300 UTC. Latent heating (including condensation, deposition, and freezing) can be seen to be dominant within a deep layer between 875 and 300 hPa with a gradual descent of the peak through the period (Fig. 13b). In common with other studies (Houze 1982; Johnson 1984), the heating peak in the convective region was located at middle levels (about 550 hPa in this case) and the magnitudes remained nearly constant throughout the developing, mature, and dissipating stages. Weak evaporational cooling occurred at low levels below 900 hPa with similar magnitudes between 0.5 and 1.0°C h^{-1}.

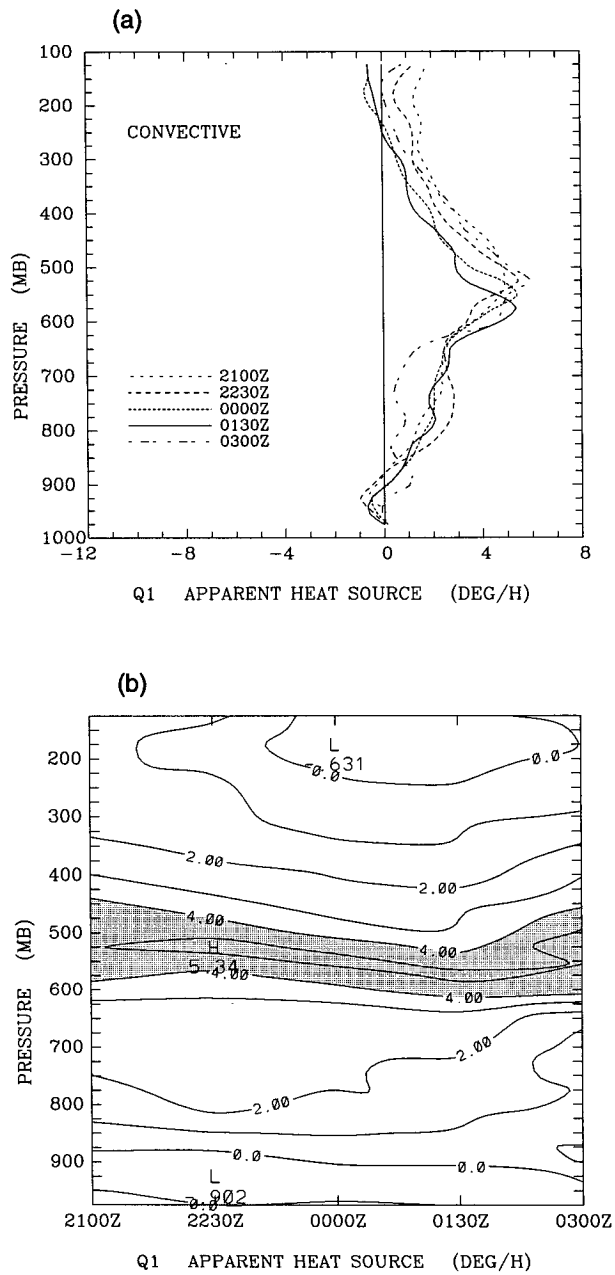

FIG. 13. Vertical profiles (a) and time series (b) of Q_1 (°C h^{-1}) averaged over the convective region of the squall line at different budget times from 2100 to 0300 UTC. Shaded area represents regions where $Q_1 > 4.0$°C h^{-1}.

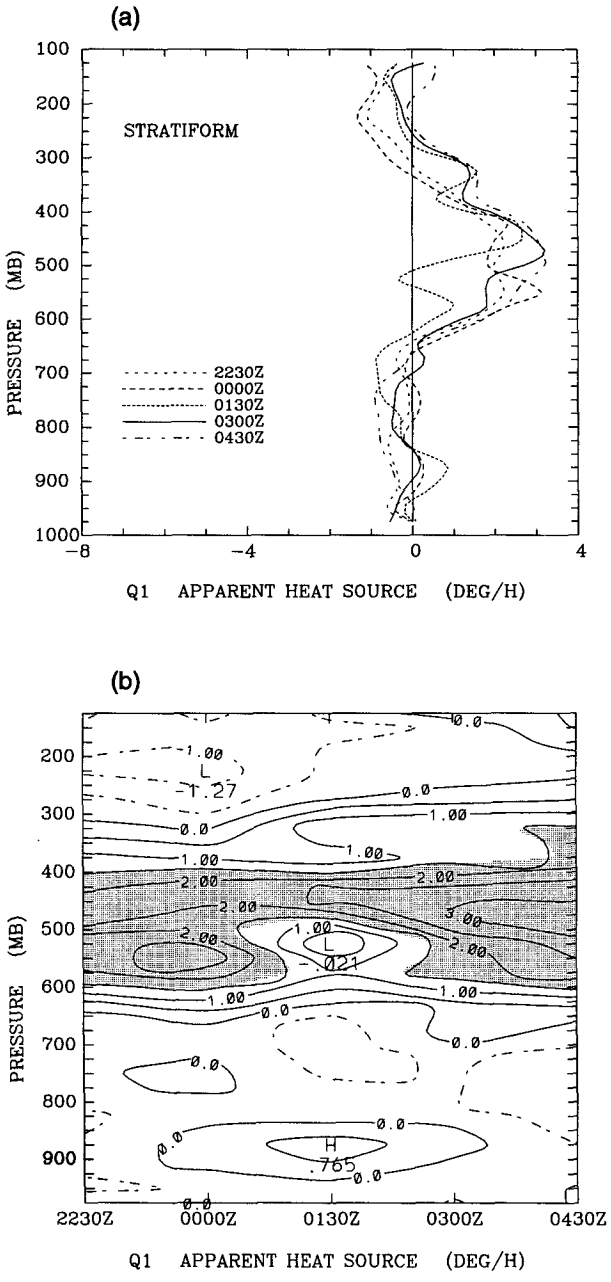

FIG. 14. Vertical profiles (a) and time series (b) of Q_1 (°C h^{-1}) averaged over the stratiform region of the squall line at different budget times from 2230 to 0430 UTC. Shaded area represents regions where $Q_1 > 1.5$°C h^{-1}

Figure 14 exhibits the vertical profiles and evolution of the Q_1 field in the stratiform region from 2230 to 0430 UTC. Heating released primarily by condensation and deposition in the mesoscale updrafts within the anvil clouds is apparent between 600 and 250 hPa. During 2230 and 0000 UTC, the peak heating was centered at about 550 hPa. At later times, coinciding with the expansion of the stratiform region, the peak shifted upward slightly and was generally located between 450 and 475 hPa. Below 650 hPa, weak cooling due to evaporation and melting can be observed with the peak centered between 700 and 800 hPa, a result similar to those determined by Houze (1982), Johnson and Young (1983), and Johnson (1984), although insufficient data under the trailing anvil and considerable

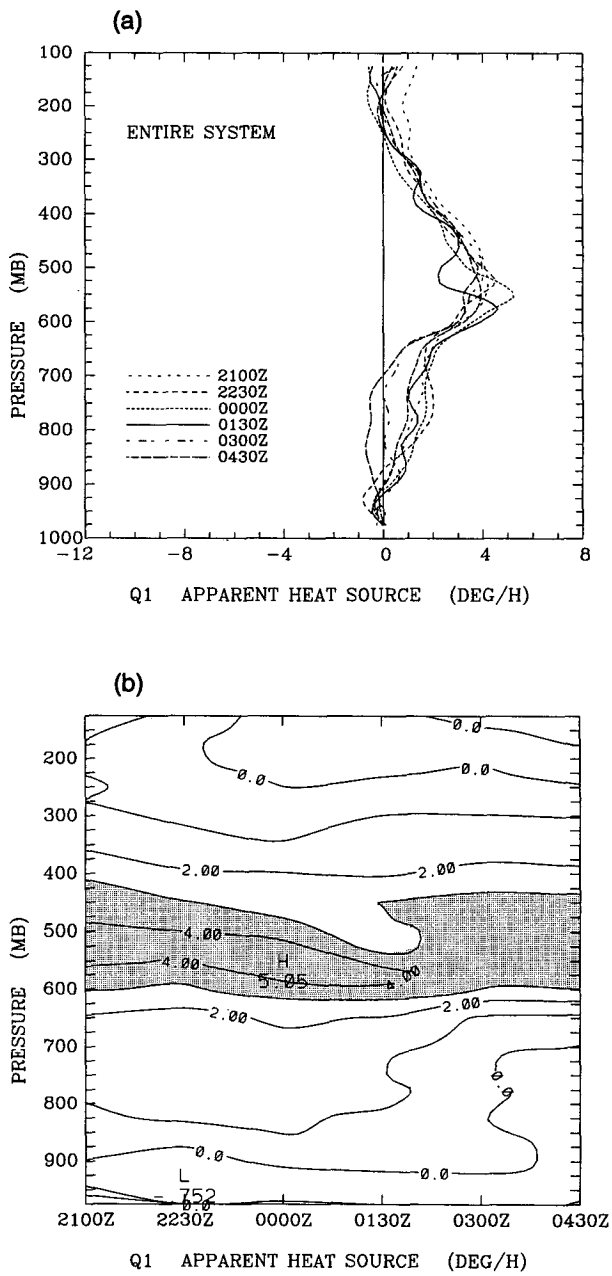

FIG. 15. Vertical profiles (a) and time series (b) of Q_1 (°C h^{-1}) averaged over the entire system of the squall line at different budget times from 2100 to 0430 UTC. Shaded area represents regions where $Q_1 > 3.0$°C h^{-1}.

aliasing from the convective region may have reduced the magnitude of the cooling.

Figure 15 shows the vertical Q_1 profiles and their evolution averaged over the entire system from 2100 to 0430 UTC. The contribution to the Q_1 profiles at early times (2100 to 0130 UTC) came mainly from the heating in the convective region. At later times (0300 to 0430 UTC), the heating rate gradually decreased and became negative between 700 and 975 hPa, which indicated increasing evaporative cooling associated with the expansion of the stratiform anvil and the weakening of the convective line. The heating peak at middle levels was still lower than those found in the 10–11 June case (Gallus and Johnson 1991) in which the stratiform region was more than three times as extensive as the convective region. In that case, the upper-level heating feature from the stratiform region dominated the system average. Another main cause for the lower vertical motion and heating peak in the 26–27 June case was probably related to the amount of instability and intensity of updrafts compared to the 10–11 June case. Johnson and Hamilton (1988) determined a value of 2300 $m^2 s^{-2}$ for the convective available potential energy at station PTT at 2230 UTC (CAPE; Moncrieff and Miller 1976; Weisman and Klemp 1982) in the 10–11 June case. In the 26–27 June case, the CAPE values were generally below 1700 $m^2 s^{-2}$ (e.g., 1675 $m^2 s^{-2}$ for station OKC at 2300 UTC 26 June).

Figure 16 compares the heating rates normalized by rainfall (Johnson 1984) for the entire system in the 26–27 June case to several other tropical and midlatitude convective systems. The three dashed lines represent the developing, mature, and dissipating stages, respectively. Curve GJ (from Gallus and Johnson 1991) was determined from the well-organized 10–11 June PRE-STORM squall line case during the late mature through decaying stages. Curve Y (from Yanai et al. 1973) and curve T (from Thompson et al. 1979) were from the tropical Pacific Marshall Islands and the tropical eastern Atlantic, respectively. The tropical cases represent composites of many MCSs. The results of this study resemble that from Gallus and Johnson (1991) except the level of peak heating is much lower in this case. The heating peak of curve Y is located at about 450 hPa, just between the curves for the two PRE-STORM cases. Curve T has a lower heating peak located at about 600 hPa, which Thompson et al. (1979) attribute to the different cloud population and lower sea surface temperatures in the GATE region. Both midlatitude studies show a pronounced effect of evaporative cooling at low levels. In the 26–27 June case, the depth of this low-level cooling progressively increased as the squall line decayed and the stratiform region expanded. In the tropics, since cloud bases are lower and the air is normally closer to saturation, evaporational cooling is smaller than in midlatitude cases. Therefore, both curves Y and T show heating at low levels instead of the weak cooling as in the PRE-STORM cases.

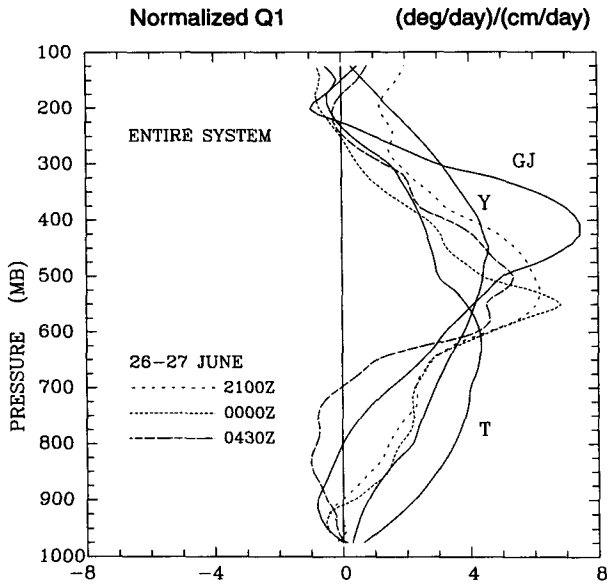

FIG. 16. Comparison of vertical Q_1 profiles normalized by the rainfall rate for average taken over the entire system (in units of K day^{-1}/1 cm day^{-1}). Curve GJ is from the 10–11 June PRE-STORM case (Gallus and Johnson 1991). Curve Y and T are from tropical Pacific islands (Yanai et al. 1973) and GATE (Thompson et al. 1979), respectively.

b. Spatial and temporal evolution of the moisture budget

Vertical cross sections for the Q_2 field at 0000 and 0430 UTC are shown in Fig. 17. At 0000 UTC (Fig. 17a) condensational drying occurred within a vertical band about 100 km wide near the leading edge, with a peak near 700 hPa. Negative values generally dominated to the rear of the system, indicating moistening due to evaporation and sublimation. At 0430 UTC (Fig. 17b), as the stratiform region expanded, a double-peak drying structure became apparent. The larger peak was located at roughly between 750 and 700 hPa near the leading edge and the second peak at 475 hPa. The maximum moistening rate (near 800 hPa) to the rear of the system increased by about 40% from 0000 to 0430 UTC.

The vertical profiles and evolution of Q_2 averaged over the entire system are illustrated in Fig. 18. During the early stages (2100 to 0000 UTC), the maximum drying rate was generally located around 700 hPa, about 150 hPa lower than the Q_1 heating peak (Fig. 15), indicative of strong deep convection (Luo and Yanai 1984). It reflects the fact that water vapor was condensed at low levels and the released heat was transported upward to midlevels by the strong convective updraft. A minor drying peak in Q_2 at middle levels may have been induced by two different mechanisms: 1) a midlevel drying feature generated by the trailing stratiform region, especially from the Kansas region, and 2) vertical eddy transport of water vapor by con-

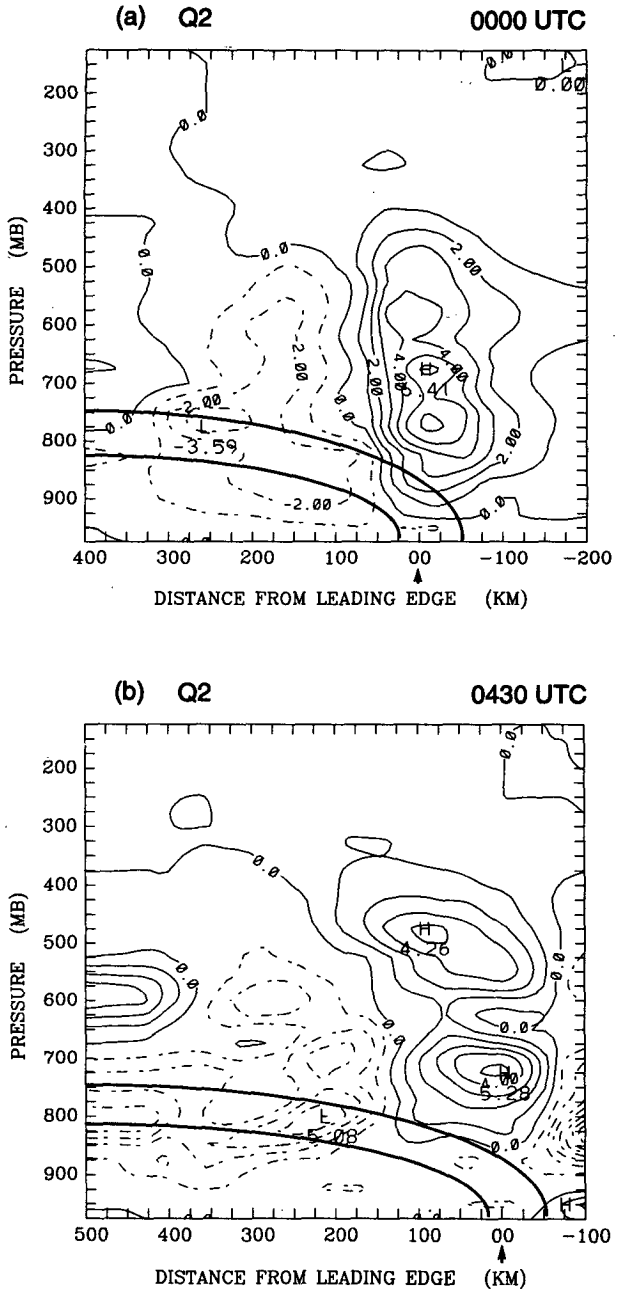

FIG. 17. Apparent moisture sink Q_2 (in °C h^{-1}) at (a) 0000 UTC, (b) 0430 UTC.

vective updrafts (Tao and Soong 1986; Dudhia and Moncrieff 1987; Lafore et al. 1988; Chong and Hauser 1990).

During the mature and dissipating stages of the squall line (0130 to 0300 UTC), a drying minimum developed between 600 to 675 hPa (Fig. 18), as was found in many tropical and midlatitude budget studies (Reed and Recker 1971; Yanai et al. 1973; Johnson 1976; Frank and McBride 1989; Gallus and Johnson 1991; Johnson and Bresch 1991). A drying peak was located at 725 hPa, and a midlevel Q_2 peak was also well developed, coincident with the radar echo and surface rainfall observations, which showed that the stratiform precipitation gradually developed and coexisted with the convective precipitation. Johnson (1984) proposed that the double-peak Q_2 structure is a result of the combination of two distinctly different drying pro-

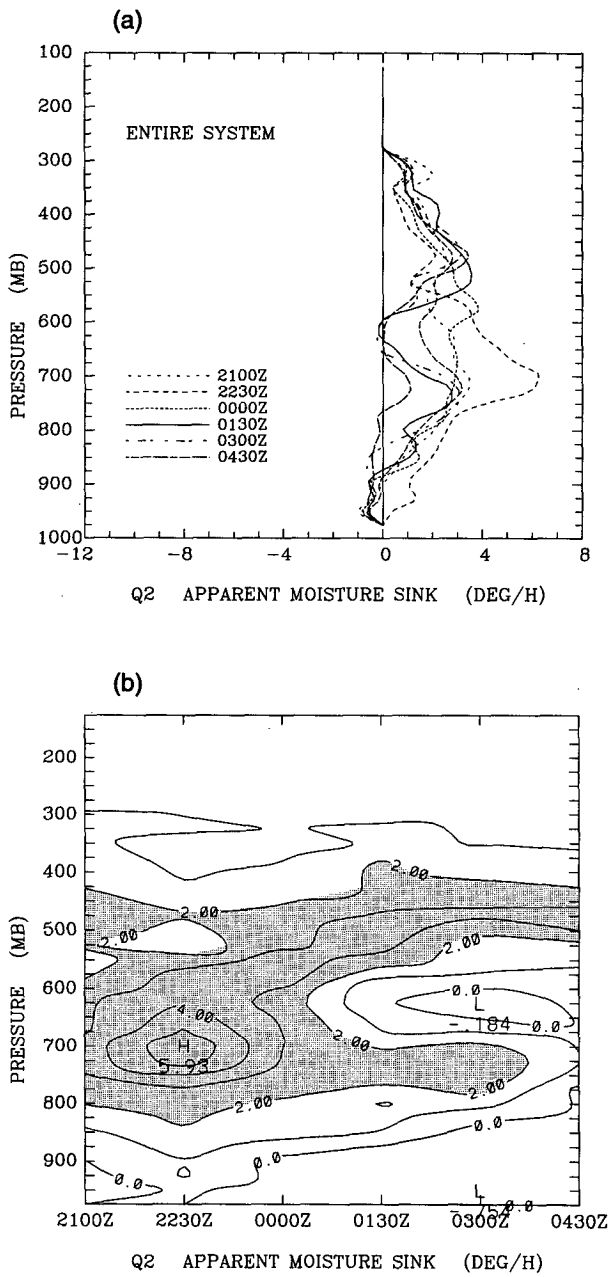

FIG. 18. Vertical profiles (a) and time series (b) of Q_2 (°C h^{-1}) averaged over the entire squall line at different budget times from 2100 to 0430 UTC. Shaded area represents regions where $Q_2 > 2.0$°C h^{-1}.

cesses. He suggested that the lower peak is a result of cumulus updrafts in the convective region, while the higher one comes from the mesoscale updrafts within anvil clouds. At 0430 UTC, the low-level drying peak gradually decreased as the convection dissipated and mesoscale moistening below anvil increased, while the midlevel drying peak remained constant. The findings in this case appear to support Johnson's hypothesis (1984) that the midlevel drying peak for the entire system, at least in its later stages, is mainly caused by the stratiform region. This result does not imply that the mechanism related to the vertical eddy transport of water vapor was not operative in the deep convection within the squall system. It just indicates that over the largest scales and lifetime of the entire squall system, the two distinct features—the convective line and the stratiform region—can contribute importantly to the double-peak Q_2 structure.

Figure 19 compares the rainfall normalized profiles of Q_2 averaged over the entire system with some other tropical and midlatitude cases. Profiles at 2230, 0130, and 0430 UTC are chosen to represent the developing, mature, and dissipating stages, respectively, in the 26–27 June case. At the developing and early mature stages (2230 UTC), the convective region dominated the contributions to the entire system average values. The single major drying peak (with a minor one near 450 hPa), which resulted from convective updrafts, was located around 700 hPa. At the mature and early dissipating stages (0130 UTC), the double-peak structure became apparent, consistent with the observation that the stratiform and convective regions coexisted. The peak drying positions were quite similar to the Y curve (Yanai et al. 1973). At 0430 UTC, the low-level drying peak decreased rapidly. Weak moistening was dominant below 750 hPa to the surface. The middle-level drying peak became prominent, coinciding with the fact that the stratiform region dominated at this time and the convective region weakened. The midlevel drying peak was located at a similar position as in the 10–11 June case (GJ curve) (Gallus and Johnson 1991).

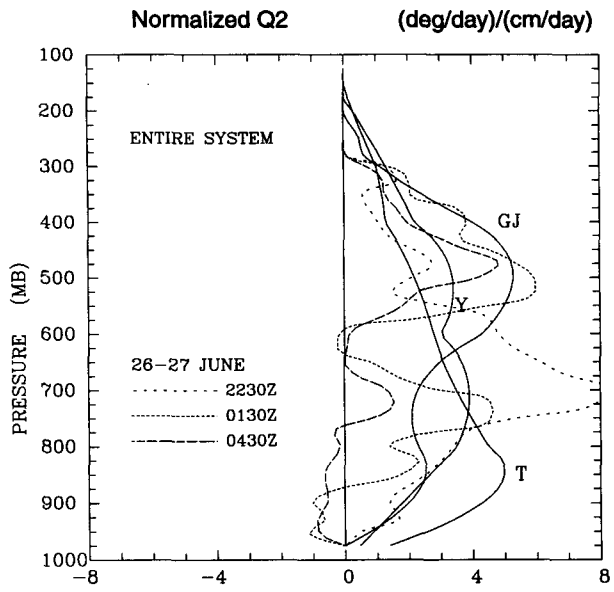

FIG. 19. Comparison of vertical Q_2 profiles normalized by the rainfall rate for average taken over the entire system (in units of K day^{-1}/1 cm day^{-1}). Curve GJ is from the 10–11 June PRE-STORM case (Gallus and Johnson 1991). Curve Y and T are from tropical Pacific islands (Yanai et al. 1973) and GATE (Thompson et al. 1979), respectively.

5. Summary and discussion

The 26–27 June PRE-STORM squall line was a slowly moving mesoscale convective system followed by a low-level cold front. It was within the sounding network for most of its evolution from the developing to mature to dissipating stages. Composited rawinsonde data have been used to investigate the evolution of the mesoscale heating, moistening, and circulation characteristics for six times at intervals of 90 minutes. Because of insufficient data, few studies have been performed over most of the life cycle of a squall line system. Similarities and differences are found compared to other midlatitude and tropical squall line cases.

Similar to the results determined from midlatitude and tropical cases, three main system-relative flows are identified within the system in the line-normal cross sections: an FTR flow extending from ahead of the leading edge to upper levels in the rear of the system, a weak surface FTR flow due to an overturning downdraft fed by divergence underneath the stratiform region, and a midlevel rear-inflow jet. There was another moderately strong RTF flow induced by a low-level cold front present at low levels behind the system, which confined the postsquall surface FTR flow within a shallow layer near the surface.

The mesoscale circulation features are found to be closely associated with the development of the stratiform region. During the developing and mature stages, the midlevel RTF flow was not apparent and remained weak well behind the squall line. At the late mature and dissipating stages as the stratiform region developed, a couplet of midlevel mesolow and mesohigh became apparent behind the convective region. The RTF flow significantly strengthened at the back edge of the squall line and extended forward into the rear of the system, suggesting that the RTF inflow jet is produced by the internal processes within the stratiform region (Smull and Houze 1987; Weisman et al. 1988; Lafore and Moncrieff 1989; Trier et al. 1991). At most times, the magnitudes of convergence reached their maximum at low levels around the leading edge, reflecting the boundary-layer feeding of mass and moisture for the system development and evolution. This convergence gradually increased from the developing to the mature stages, and then slowly decreased during the dissipat-

ing stage. At midlevels behind the convective region, convergence generally increased from the developing and mature all the way to the dissipating stages, suggesting that the influence of the stratiform region increased. The system rear inflow gradually strengthened and developed forward, converging more intensively with the opposing FTR flow and supplying more mass to the developing mesoscale downdraft in the stratiform region. From the vorticity balance perspective of Rotunno et al. (1988), it can be argued that the cold pool circulation then overwhelmed the ambient vertical shear and the system tilted upshear. These findings are consistent with the modeling studies of Lafore and Moncrieff (1989) and Weisman (1992).

During the early developing stage, a narrow vertical band of upward motion corresponding to a narrow convective line was present around the leading edge over Oklahoma. Moderately strong compensating downward motion occurred ahead of and behind the system. A wide band of upward motion was noticed over Kansas where stratiform and convective regions coexisted. The intensity of upward motion within the system gradually increased and reached a maximum at the mature stage. During the decaying stage, the upward motion weakened and the upshear tilting of the system gradually increased as the stratiform region developed. To the rear of the system, strong downward motion was evident and extended into the low levels of the system.

The system-averaged heating (Q_1) peak was generally located at middle levels between 500 and 550 hPa throughout the developing and mature to the dissipating stages, considerably lower than in the 10–11 June PRE-STORM squall line (400 hPa) (Gallus and Johnson 1991). The lower heating peak in the 26–27 June case was likely a consequence of lower values of CAPE and a weaker and less extensive region of stratiform precipitation.

The moisture budget clearly showed the contribution from the convective and stratiform regions at different stages. During the developing and early mature stages, a single drying peak (positive Q_2) was present at low levels around 700 hPa, much lower than the peak heating level, suggestive of a dominance of deep convective activity. A minor secondary peak in Q_2 was observed in the midtroposphere at this time. The double-peak structure in Q_2 at this time may have been induced by two different mechanisms: 1) a midlevel drying feature generated by the trailing stratiform region, especially over the Kansas region, and 2) vertical eddy transport of water vapor within the convective region, as proposed by Dudhia and Moncrieff (1987) and Lafore et al. (1988). During the late mature and dissipating stages, a double-peak structure became very prominent as the stratiform region became well developed. The midlevel drying peak was located at 475 hPa with a weak moistening region separating it from the low-level drying peak. The magnitudes of the midlevel drying peak remained nearly constant at later stages while the low-level drying peak gradually weakened with time. It is believed that the double-peak Q_2 structure for the entire system during the late mature and decaying stage was mainly a consequence of the coexistence of two features: an expanding stratiform region and a weakening convective line, although the divergence of the vertical eddy flux of water vapor may have also contributed to this feature.

In this study the heat and moisture budgets and mesoscale circulation features of a midlatitude frontal squall line have been investigated through most of its life cycle. Many mesoscale features (strengthening of the midlevel RTF flow, a couplet of midlevel mesolow and mesohigh, midlevel convergence maximum, etc.) were found to be closely related to the development of the stratiform region. Further research is under way on the evolution of the secondary circulation, frontogenesis, and the role of the low-level cold front as the stratiform region developed.

Acknowledgments. The authors want to thank Dr. Bradley F. Smull and Robert A. Hueftle of NOAA/National Severe Storm Laboratory for helping in generating radar maps. The helpful comments of Scott Braun and two anonymous reviewers are appreciated. This research has been supported by the National Science Foundation, Atmospheric Sciences Division, under Grants ATM-9013112.

REFERENCES

Augustine, J. A., and E. J. Zipser, 1987: The use of wind profilers in a mesoscale experiment. *Bull. Amer. Meteor. Soc.*, **68**, 4–17.

Balsley, B. B., W. L. Ecklund, D. A. Carter, A. C. Riddle, and K. S. Gage, 1988: Average vertical motions in the tropical atmosphere observed by a radar wind profiler on Pohnpei (7°N latitude, 157°E longitude). *J. Atmos. Sci.*, **45**, 396–405.

Barnes, S. L., 1964: A technique for maximizing details in numerical weather map analysis. *J. Appl. Meteor.*, **3**, 396–409.

Biggerstaff, M. I., and R. A. Houze, Jr., 1991: Midlevel vorticity structure of the 10–11 June 1985 squall line. *Mon. Wea. Rev.*, **119**, 3066–3079.

Chong, M., and D. Hauser, 1990: A tropical squall line observed during the COPT 81 experiment in west Africa. Part III: Heat and moisture budgets. *Mon. Wea. Rev.*, **118**, 1696–1706.

——, P. Amayenc, G. Scialom, and J. Testud, 1987: A tropical squall line observed during the COPT 81 experiment in west Africa. Part I: Kinematic structure inferred from dual-Dopplar radar data. *Mon. Wea. Rev.*, **115**, 670–694.

Dudhia, J., and M. W. Moncrieff, 1987: A numerical simulation of quasi-stationary tropical convective bands. *Quart. J. Roy. Meteor. Soc.*, **113**, 929–967.

Fankhauser, J. C., 1974: The derivation of consistent fields of wind and geopotential height from rawinsonde data. *J. Appl. Meteor.*, **13**, 637–646.

Frank, W. M., and J. L. McBride, 1989: The vertical distribution of heating in AMEX and GATE cloud clusters. *J. Atmos. Sci.*, **46**, 3464–3478.

Gallus, W. A., Jr., and R. H. Johnson, 1991: Heat and moisture budgets of an intense midlatitude squall line. *J. Atmos. Sci.*, **48**, 122–146.

Gamache, J. F., and R. A. Houze, Jr., 1982: Mesoscale air motions associated with a tropical squall line. *Mon. Wea. Rev.*, **110**, 118–135.

Hamilton, R. A., and J. N. Archbold, 1945: Meteorology of Nigeria and adjacent territory. *Quart. J. Roy. Meteor. Soc.*, **71**, 231–262.

Houze, R. A., Jr., 1977: Structure and dynamics of a tropical squall-line system. *Mon. Wea. Rev.*, **105**, 1540–1567.

——, 1982: Cloud clusters and large-scale vertical motions in the tropics. *J. Meteor. Soc. Japan*, **60**, 396–409.

——, 1989: Observed structure of mesoscale convective systems and implications for large-scale heating. *Quart. J. Roy. Meteor. Soc.*, **115**, 425–461.

——, C. A. Leary, and J. F. Gamache, 1980: Diagnosis of cloud mass and heat fluxes from radar and synoptic data. *J. Atmos. Sci.*, **37**, 754–773.

——, B. F. Smull, and P. Dodge, 1990: Mesoscale organization of springtime rainstorms in Oklahoma. *Mon. Wea. Rev.*, **118**, 613–654.

Johnson, R. H., 1976: The role of convective-scale precipitation downdrafts in cumulus and synoptic-scale interactions. *J. Atmos. Sci.*, **33**, 1890–1910.

——, 1980: Diagnosis of convective and mesoscale motion during Phase III of GATE. *J. Atmos. Sci.*, **387**, 733–753.

——, 1984: Partitioning tropical heat and moisture budgets into cumulus and mesoscale components: Implication for cumulus parameterization. *Mon. Wea. Rev.*, **112**, 1590–1601.

——, and G. S. Young, 1983: Heat and moisture budgets of tropical mesoscale anvil clouds. *J. Atmos. Sci.*, **40**, 2138–2147.

——, and P. J. Hamilton, 1988: The relationship of surface pressure features to the precipitation and airflow structure of an intense midlatitude squall line. *Mon. Wea. Rev.*, **116**, 1444–1472.

——, and J. F. Bresch, 1991: Diagnosed characteristics of Mei-Yu precipitation systems over Taiwan during the May–June 1987 TAMEX. *Mon. Wea. Rev.*, **119**, 2540–2557.

——, W. A. Gallus, Jr., and M. D. Vescio, 1990: Near-tropopause vertical motion within the trailing stratiform region of a midlatitude squall line. *J. Atmos. Sci.*, **47**, 2200–2209.

Klimowski, B. A., 1994: Initiation and development of rear inflow within the 28–29 June 1989 North Dakota mesoconvective system. *Mon. Wea. Rev.*, **122**, 765–779.

Kuo, Y.-H., and R. A. Anthes, 1984: Accuracy of diagnostic heat and moisture budgets using SESAME-79 field data as revealed by observing system simulation experiments. *Mon. Wea. Rev.*, **112**, 1465–1481.

Lafore, J.-P., and M. W. Moncrieff, 1989: A numerical investigation of the organization and interaction of the convective and stratiform regions of tropical squall lines. *J. Atmos. Sci.*, **46**, 521–544.

——, J.-L. Redelsperger, and G. Jaubert, 1988: Comparison between a three-dimensional simulation and Doppler radar data of a tropical squall line: Transports of mass, momentum, heat, and moisture. *J. Atmos. Sci.*, **45**, 3483–3500.

Leary, C. A., and R. A. Houze, Jr., 1979: The structure and evolution of convection in a tropical cloud cluster. *J. Atmos. Sci.*, **36**, 437–457.

——, and ——, 1980: The contribution of mesoscale motions to the mass and heat fluxes of an intense tropical convective system. *J. Atmos. Sci.*, **37**, 784–796.

Lin, X., 1992: A diagnostic study of a midlatitude frontal squall line. Paper 510, Dept. of Atmospheric Science, Colorado State University, Ft. Collins, CO 80523, 141 pp.

Luo, H., and M. Yanai, 1984: The large-scale circulation and heat sources over the Tibetan plateau and surrounding areas during the early summer of 1979. Part II: Heat and moisture budgets. *Mon. Wea. Rev.*, **112**, 966–989.

Moncrieff, M. W., and M. J. Miller, 1976: The dynamics and simulation of tropical cumulonimbus and squall lines. *Quart. J. Roy. Meteor. Soc.*, **102**, 373–394.

Newton, C. W., 1950: Structures and mechanisms of the prefrontal squall line. *J. Meteor.*, **7**, 210–222.

Nitta, T., 1972: Energy budget of wave disturbance over the Marshall Islands during the years of 1956 and 1958. *J. Meteor. Soc. Japan*, **50**, 71–84.

O'Brien, J. J., 1970: Alternative solutions to the classical vertical velocity problem. *J. Appl. Meteor.*, **9**, 197–203.

Ogura, Y., and M. T. Liou, 1980: The structure of a mid-latitude squall line. A case study. *J. Atmos. Sci.*, **37**, 553–567.

——, and D. Portis, 1982: Structure of the cold front observed in SESAME-AVE III and its comparison with the Hoskins–Bretherton frontogenesis model. *J. Atmos. Sci.*, **39**, 2773–2792.

Reed, R. J., and E. E. Recker, 1971: Structure and properties of synoptic-scale wave disturbances in the equatorial western Pacific. *J. Atmos. Sci.*, **28**, 1117–1133.

Rotunno, R., J. B. Klemp, and M. L. Weisman, 1988: A theory for strong, long-lived squall lines. *J. Atmos. Sci.*, **45**, 463–485.

Rutledge, S. A., R. A. Houze, Jr., M. I. Biggerstaff, and T. Matejka, 1988: The Oklahoma–Kansas mesoscale convective system of 10–11 June 1985: Precipitation structure and single-Doppler radar analysis. *Mon. Wea. Rev.*, **116**, 1409–1430.

Sanders, F., and R. J. Paine, 1975: The structure and thermodynamics of an intense mesoscale convective storm in Oklahoma. *J. Atmos. Sci.*, **32**, 1563–1579.

Schmidt, J. M., and W. R. Cotton, 1990: Interaction between upper and lower tropospheric gravity waves on squall line structure and maintenance. *J. Atmos. Sci.*, **47**, 1205–1222.

Smull, B. F., and R. A. Houze, Jr., 1985: A midlatitude squall line with a trailing region of stratiform rain: Radar and satellite observations. *Mon. Wea. Rev.*, **113**, 117–133.

——, and ——, 1987: Rear inflow in squall lines with trailing stratiform precipitation. *Mon. Wea. Rev.*, **115**, 2869–2889.

Srivastava, R. C., T. J. Matejka, and T. J. Lorello, 1986: Doppler radar study of the trailing anvil region associated with a squall line. *J. Atmos. Sci.*, **43**, 356–377.

Stumpf, G. J., R. H. Johnson, and B. F. Smull, 1991: The wake low in a midlatitude mesoscale convective system having complex organization. *Mon. Wea. Rev.*, **119**, 134–158.

Tao, W.-K., and S.-T. Soong, 1986: A study of the response of deep tropical clouds to mesoscale processes: Three-dimensional numerical experiments. *J. Atmos. Sci.*, **43**, 2653–2676.

Thompson, R. M., Jr., S. W. Payne, E. E. Recker, and R. J. Reed, 1979: Structure and properties of synoptic-scale wave disturbances in the intertropical convergence zone of the eastern Atlantic. *J. Atmos. Sci.*, **36**, 53–72.

Trier, S. B., D. B. Parsons, and J. H. E. Clark, 1991: Environment and evolution of a cold-frontal mesoscale convective system. *Mon. Wea. Rev.*, **119**, 2429–2455.

Weisman, M. L., 1992: The role of convectively generated rear-inflow jets in the evolution of long-lived mesoconvective systems. *J. Atmos. Sci.*, **49**, 1826–1847.

——, and J. B. Klemp, 1982: The dependence of numerically stimulated convective storms on vertical wind shear and buoyancy. *Mon. Wea. Rev.*, **110**, 504–520.

——, ——, and, R. Rotunno, 1988: Structure and evolution of numerically simulated squall line. *J. Atmos. Sci.*, **45**, 1990–2013.

Yanai, M., S. Esbensen, and J. H. Chu, 1973: Determination of bulk properties of tropical cloud clusters from large-scale heat and moisture budgets. *J. Atmos. Sci.*, **30**, 611–627.

Zhang, D.-L., and K. Gao, 1989: Numerical simulation of an intense squall line during 10–11 June 1985 PRE-STORM. Part II: Rear inflow, surface pressure perturbations, and stratiform precipitation. *Mon. Wea. Rev.*, **117**, 2067–2094.

Zipser, E. J., 1977: Mesoscale and convective-scale downdrafts as distinct components of squall-line structure. *Mon. Wea. Rev.*, **105**, 1568–1589.

——, 1988: The evolution of mesoscale convective systems: Evidence from radar and satellite observation. *Tropical Rainfall Measurements*, J. S. Theon and N. Fugono, Eds., A. Deepak, 159–166.